Improvement of the Analysis Strategy of GEONET

Yuki Hatanaka, Toyohisa Iizuka, Masanori Sawada, Atsushi Yamagiwa, Yukie Kikuta, James M. Johnson,[1] Christian Rocken[1]

Abstract

A new analysis strategy of the GPS Earth Observation NETwork (GEONET) of the Geographical Survey Institute (GSI), Japan, was proposed by taking into account improved models and methods. The routine analysis system was upgraded and reanalysis of the data of the past five years of GEONET was carried out applying the new analysis strategy. Comparison of the new and old solutions shows that the quality of the solutions is quite uniform for the entire period and the root mean square coordinates are reduced by about 50 % after removing the linear and seasonal trends and the event offsets. The improvement of the precision of the vertical component provides us more opportunities for interpretations of the vertical crustal deformations.

1. Introduction

The routine solutions of GEONET have been utilized to detect many kinds of geophysical phenomena such as coseismic crustal deformation (e.g. Tsuji *et al*., 1995, Hashimoto *et al*., 1996), the steady state crustal deformation (e.g. Miyazaki and Heki, 2001), and variation of water vapor distribution (Iwabuchi *et al*., 2000). Recently, more detailed features such as slow earthquake (e.g. Ozawa *et al*., 2001) and seasonal variation (Murakami and Miyazaki, 2001; Heki, 2001) have been discussed using the routine solutions of GEONET. The requirement for the accuracy of the GEONET solution is thereby becoming higher and higher.

On the other hand, it has become clear that there are several problems in GEONET analyses; distortion of phase characteristics by radomes and monument multipath (Hatanaka *et al*., 2001a,b) and weakness of network configuration (Hatanaka, 2003). These problems affect the scatter and the seasonal signals/noises of the solutions and it is inferred that the seasonal signals contain a certain number of artifacts.

The change in the analysis strategy is also a problem. Several changes have been made to the analysis strategy of GEONET since the establishment of the GEONET system in 1996. For example, the ITRF96 coordinates and velocities were adopted in January, 2000. Site velocity had not been taken into account until then. The Ashtech sub-network, which had consisted of a single cluster, was divided into two regional clusters at the same time (i.e. in January, 2000). The new phase maps have been applied since January 23, 2001. Because of these changes, the quality of the routine solutions was not uniform and there were discontinuities in the time series of coordinates and baseline components. The inhomogeneity of the solutions, together with the individual error sources, has been a large barrier to interpreting any solutions across these periods.

In this paper, we propose an improved analysis strategy in which known problems are fixed and the updated models are taken into account. The routine analysis system is then revised by applying the new analysis strategy. The data for the past five years are reanalyzed with the improved strategy to get solutions with uniform quality.

In the following, the analysis strategy used previously is referred as the old (analysis) strategy, and the newly proposed one is referred as the new (analysis) strategy. Similarly, the solutions obtained by the old and new strategies are referred to as the old and new solutions, respectively.

2. Overview of GEONET

GEONET is a nationwide GPS permanent array

[1] University Corporation for Atmospheric Research/GPS Science and Technology

established by GSI to monitor crustal deformations and to provide reference stations for land surveying by GPS. It covers the whole area of Japan with 947 continuous permanent GPS stations as of June 2002. The mean distance between the stations is about 25 kilometers (Fig. 1).

GEONET has been built up in several steps. GSI installed 110 stations in the southern Kanto and Tokai areas from 1993 to 1994 to monitor crustal deformations. This network was called the Continuous Strain Monitoring System with GPS by GSI (COSMOS-G2; Sagiya *et al*., 1995). In 1994, 100 continuous GPS stations were installed to cover the whole of Japan except for the southern Kanto and Tokai areas where the COSMOS-G2 network was already in operation. This network was named GRAPES (GPS Regional Array for Precise Surveying/Physical Earth Science; Miyazaki *et al*., 1996). Just after the start of the operation of GRAPES at the beginning of October, 1994, large earthquakes took place around Japan; the Hokkaido-Toho-Oki earthquake (October 4, 1994, M8.1), the Sanriku-Haruka-Oki earthquake (December 28, 1994, M7.5), and the Hyougoken-Nanbu earthquake (also called the Kobe earthquake; January 17, 1995, M7.2). Co-seismic crustal deformations were clearly detected by GRAPES for all these earthquakes (Tsuji, *et al*., 1995; Hatanaka *et al*., 1995; Hashimoto *et al*., 1996). The timely and precise results of GRAPES demonstrated the advantage and effectiveness of permanent GPS networks for monitoring crustal deformations, and the reinforcement of the network was approved. In 1995, the two separate systems COSMOS-G2 and GRAPES were integrated and an additional 400 stations were established (Miyazaki *et al*., 1997). The operation of the integrated network, named the GPS Earth Observation Network (GEONET), started in March, 1996. Since then, 337 stations have been added, and this network has been operated until now with occasional modifications.

The specification of the observation stations is not uniform because of the historical background of the network. Three types of antenna/receiver systems are used and there are at least four different types of monument, with several exceptions (Fig. 2). GPS antennas are

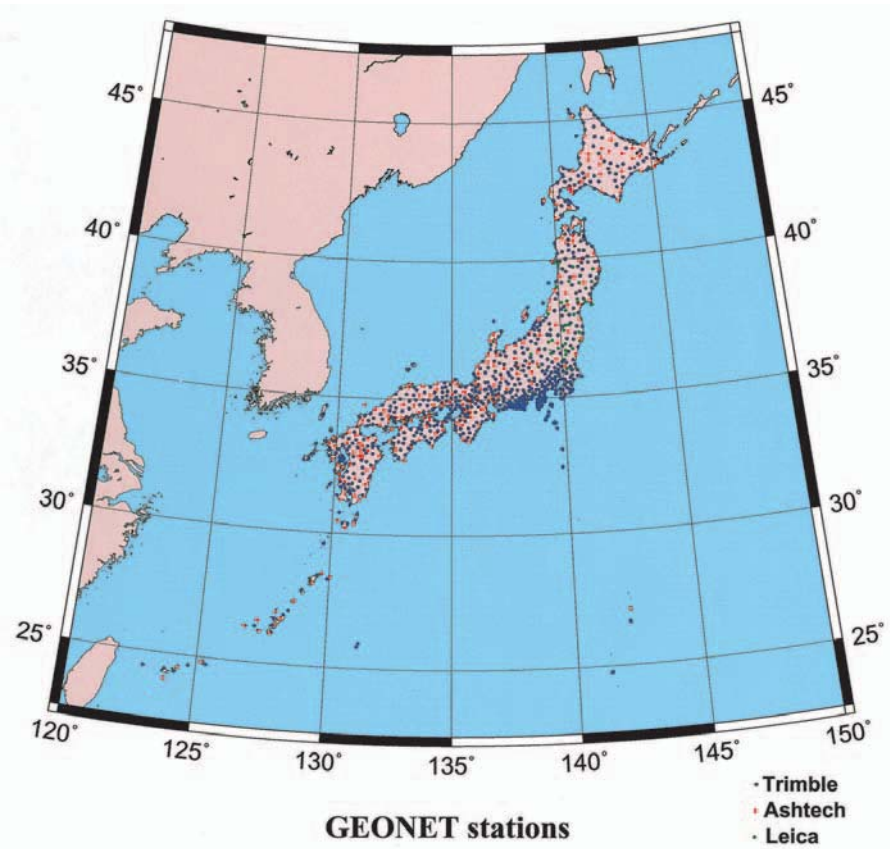

Fig. 1 Geographical distribution of GEONET stations as of 2002. The stations are classified into the three sub-networks by the antenna and receiver types: Trimble (blue), Ashtech (red) and Leica (green).

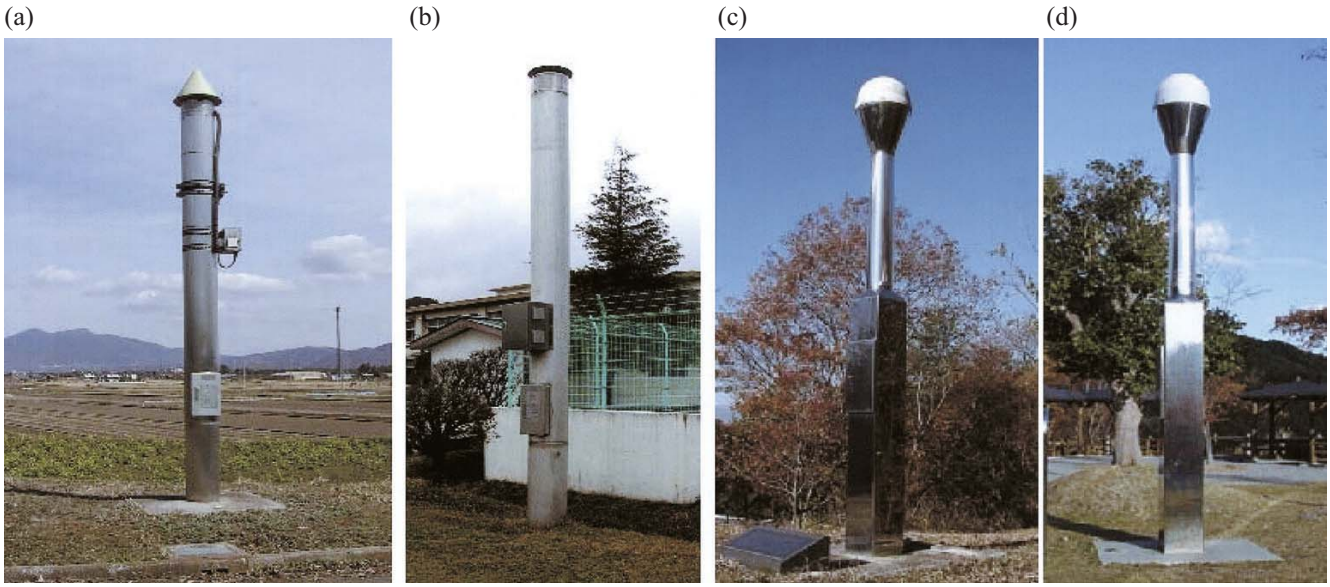

Fig. 2 Monumentation of typical GEONET stations. (a) Type 93 with conical radome, 92110(TSUKUBA), (b) Type 93 without radome, 93037(ICHIHARA2), (c) Type 94, 940029 (MIZUSAWA), and (d) Type 95, 950171(OOFUNATO).

installed at the top of 5 meter tall stainless steel pillars with a two meter deep concrete bases. The antennas are covered with radomes at all but 100 stations. A GPS receiver, communication equipment and a backup battery are settled in the pillar at each station. 120 of the stations are equipped with tiltmeters to confirm the stability of the pillars at the time of seismic events.

Each receiver records GPS signals continuously with a sampling interval of 30 seconds and an elevation mask of 15 degrees. Data for 10 days can be stored on site to assure data availability even if data communications are lost by accident. The data observed at each station are transferred to GSI in Tsukuba once per day by public telephone lines. The data are converted into the RINEX format (Gurtner and Mader, 1990) and stored in a database.

The data are analyzed routinely in two ways. First, quick solutions are calculated by using "combined orbit information" which is a combination of rapid and predicted orbit information provided by the Center of Orbit Determination in Europe (CODE), Astronomical Institute, University of Berne. After publication of the International GPS Service (IGS) final orbits two weeks after the observation, the final solutions of GEONET are calculated using them. The analysis software packages BERNESE (Hugentobler, *et al*., 2001), GIPSY (Webb and Zumberge, 1993) and GAMIT/GLOBK (King and Bock, 1993) can be used in GEONET. Currently BERNESE is used routinely. Results of the analyses are also stored in the database.

3. The Changes of the Analysis Strategies

The specification of the new analysis strategy is summarized in the Appendix. In the succeeding sections, I will make comments on the changes from the old strategy to the new one, which are listed in Table 1.

3.1 New Phase Maps Specific for Antenna-Monument Types

Since several types of antennas are used in the network, it was anticipated that there would be biases in the baseline solutions among stations with different antennas due to the mis-modeling of antenna phase characteristics. Antenna phase characteristics were corrected with phase maps, which were antenna-specific models of phase center variations (PCV). However, the phase maps for the antenna types used in GEONET were not available at the beginning of the operation. The phase maps for other antenna types that were provided by IGS were substituted for GEONET sites; i.e. TRM14532.00 instead of TRM23903.00, ASH700228A instead of ASH700718A, and AOAD/M_T instead of LEIAT303. To minimize these problems, the network was divided into three sub-networks so that the antenna types were uniform within each sub-network. Differences in monumentation such as radomes or antenna mount, however, have not

Table 1 The list of the changes of the analysis strategy

	The old strategy	The new strategy
Software	BERNESE Ver. 4.1	BERNESE Ver. 4.2
Solid earth tide	Constant Love number	Dependency of Love numbers on frequency is taken into account.
Pole tide	Not applied	IERS conventions, 1996
Subdaily polar motion	Not applied	Ray model (Ray, 1994)
Ocean loading correction	Not applied	Matsumoto *et al*. (2000)
Site phase characteristics	Dependency of monument type is not taken into account.	Specific for the antenna and monument types (Hatanaka *et al*., 2001a).
Troposphere estimation model and strategy	Hydrostatic delay is corrected by the Saastamoinen (1973) model, and zenith wet delay is estimated with the mapping function of the simplified Hopfield model (Wells, 1974).	Hydrostatic delay is corrected by the zenith delay calculated by the Saastamoinen (1973) model and Niell's (1996) mapping function (NMF) for the dry term, and zenith wet delay is estimated by the NMF for wet term.
Network configuration	Not tuned. The cluster division is not the uniform for the entire period.	Modified according to Hatanaka (2003).
Coordinates of the fixed stations	Obtained from local tie from IGS site (TSKB). Site velocity is not taken into account for 1996-1999. The coordinates and velocity of ITRF94 are applied for 2000-2001.	Obtained from local tie from IGS site (TSKB) based on the ITRF97 coordinates and velocity.
Reference frame of orbit information	ITRF94, ITRF96, ITRF97	Transformed into ITRF97

received much attention until recently.

Hatanaka *et al*. (2002a) found that both the phase characteristics of radomes and the multipath from the metal plate at the top of the station pillars distort the antenna phase characteristics, and significantly affected solutions. They obtained phase maps which include these effects by a phase calibration experiment. The biases of the coordinates (height bias of 10 cm or more, scale bias up to 20 ppb) were eliminated, and the standard deviation (S.D.) of the vertical coordinates was reduced by 6.1 % by applying the new phase maps (Hatanaka *et al*., 2002b). These new phase maps are adopted in the new analysis strategy.

The change of the phase maps also affects the local tie of the constrained sites to the IGS site at Tsukuba. This issue will be dealt with in Section 3.4 together with the issue of reference frame.

3.2 Ocean Loading Tide Model

Until recently, ocean loading displacement was not always modeled by GPS analysis software packages. This is also the case with the old routine analysis of GEONET. However, the amplitude of the ocean loading displacement is of the level of several centimeters in the Japanese island area, so these signals should be taken into account. Precise models of ocean tide loading are provided nowadays. Hatanaka *et al*. (2001c) evaluated the model proposed by Matsumoto *et al*. (2000, 2001) by applying it to the GEONET analysis (Fig. 3) and showed that this model explains about 71 % of the power of the tidal amplitudes in the variation of the subdaily coordinates, except for the K_1 and K_2 constituents. Although the ocean loading displacement is mostly averaged out for daily coordinates, it impacts on the GPS tropospheric delay estimates since the modeling errors especially of the vertical tidal displacement are highly correlated to the tropospheric parameters (Fig. 4).

The amplitudes and phases of the ocean tide loading displacement for the 11 major tidal constituents (M_2, S_2, Q_2, K_2, K_1, N_1, O_1, P_1, M_f, M_m, S_{sa}) are applied at each station in the new analysis strategy. These parameters are calculated by the GOTIC2 software (Matsumoto *et al*., 2001) by using the fourth-order mesh data of land-sea distribution.

3.3 Network configuration

Hatanaka (2003) examined results of a test analysis of GEONET data, and found that defects of clustering configurations of GPS networks have a significant impact on the stability of the combined solutions. Four kinds of

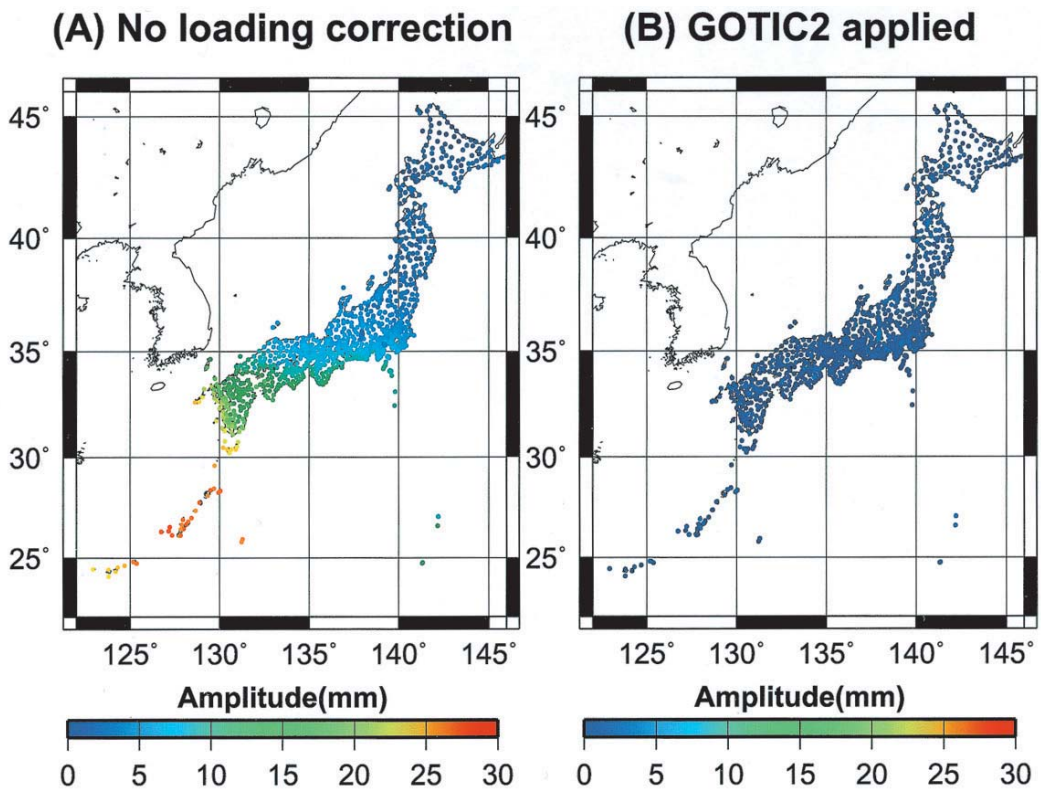

Fig 3 Distribution of amplitude of M2 period signals in vertical coordinates without ocean loading corrections (A) and with the ocean loading correction by GOTIC2 model (B).

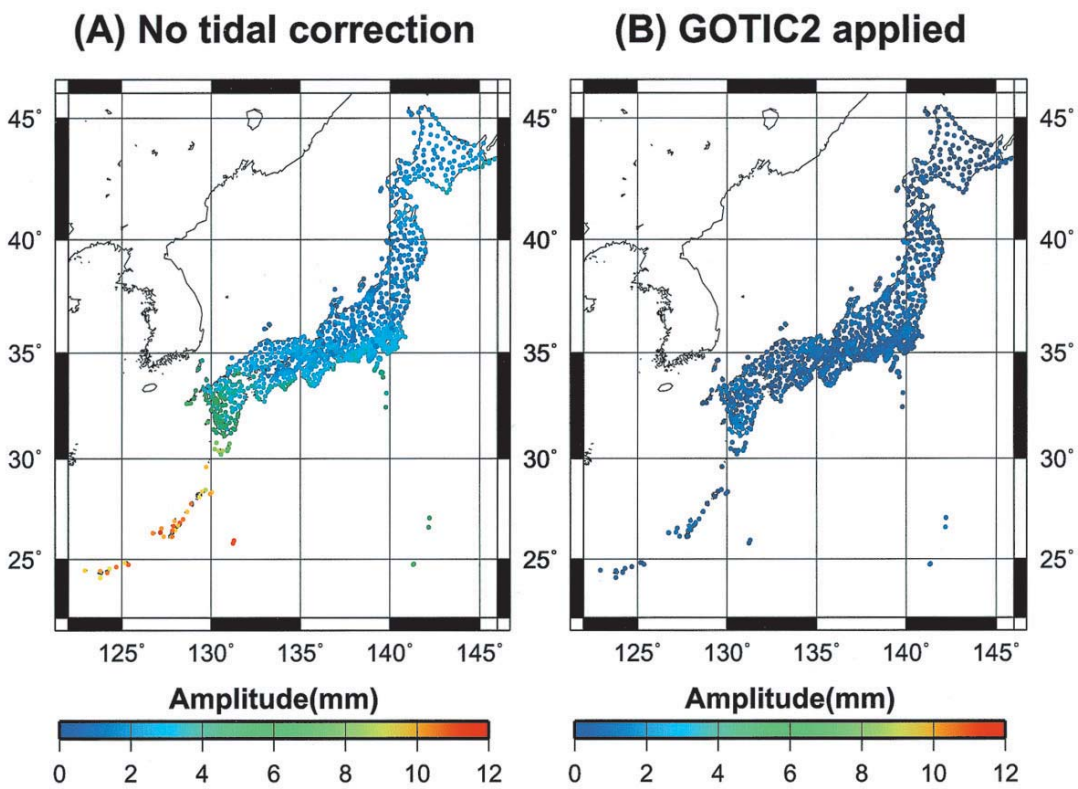

Fig. 4 Amplitude of M2 period signals in tropospheric delay estimates without ocean loading corrections (A) and that with the ocean loading corrections by GOTIC2 model (B).

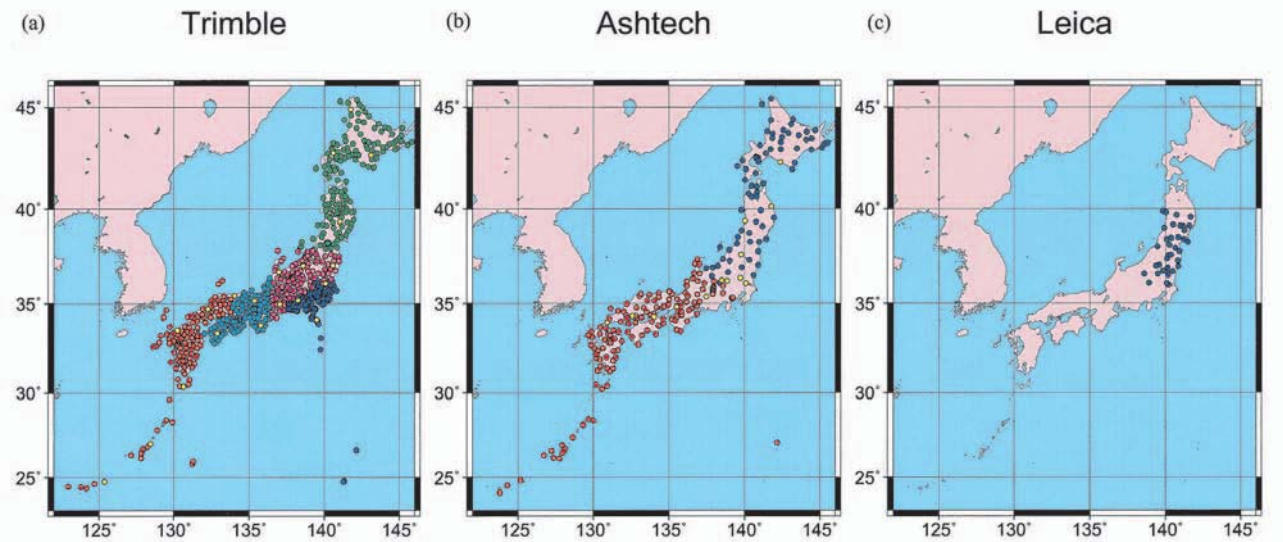

Fig. 5 Site distribution of the regional clusters of (a) Trimble sub-network, (b) Ashtech sub-network, and (c) Leica sub-network. Stations of different clusters are plotted with a different color. Yellow circles in (a) show the backbone stations, and those in (b) show the stations that are common to the two clusters.

factors are involved and magnify the biases and scatter of the solutions; constraint of fiducial-free solutions arose from fixed satellite orbits, systematic error in the fiducial-free solutions, imbalance of data weight, and weakness of connectivity of the sub-networks and clusters.

The above problem was effectively removed by improving the connectivity of the network with a careful choice of network nodes. The improved network configuration proposed by Hatanaka (2003) is adopted for the new analysis strategy (Fig. 5). This change is supposed to reduce 30 % of the variance of the height component.

3.4 Coordinates and Velocity of Stations to be Constrained

A reference frame is introduced in two ways in the GEONET solutions; one is through the coordinates of constrained sites and the other is through satellite orbit information and earth rotation parameters. The latter will be discussed in the next subsection.

The whole network is divided into 3 sub-networks according to the receiver types. Each of the sub-networks contains a station in Tsukuba whose coordinates are heavily constrained to the values derived from the a priori coordinates and velocity. Therefore there are three fiducial stations in Tsukuba. The a priori coordinates and velocity of the constrained stations are calculated by analyzing the baselines between each of these stations and the Tsukuba IGS site (TSKB). The baselines are analyzed with the single frequency L1 without estimating the tropospheric delay because the lengths of the baselines are short (less than 56 meters). The new phase maps obtained (Hatanaka, 2002a) are applied.

In principle, the above procedure introduces ITRF into the solution of the whole network because the coordinates and velocity of TSKB are given in ITRF. In the old analysis strategy, however, this was not true in a strict sense. First, the old phase maps were not used for analyzing local tie vectors as discussed in Hatanaka *et al.* (2001b). Because the solutions obtained by using the old phase maps are biased and the biases are dependent on analysis strategy, the local tie vectors obtained by L1 signals without estimating tropospheric parameters are not consistent with the network solutions obtained by using the linear combination of dual frequencies with estimating tropospheric parameters. The definition of coordinates is ambiguous in the old solutions because of this problem. Second, the site velocity was not taken into account when the routine analysis of GEONET started in 1996. This situation continued until the beginning of 2001 because the change in analysis settings could cause discontinuity in the coordinate time series and it is troublesome for the monitoring of crustal deformation. The site velocity was introduced in 2001, and the reference frame of the a priori coordinates was switched from ITRF94 to ITRF96 at the same time. The data after January 1, 2000 was reanalyzed

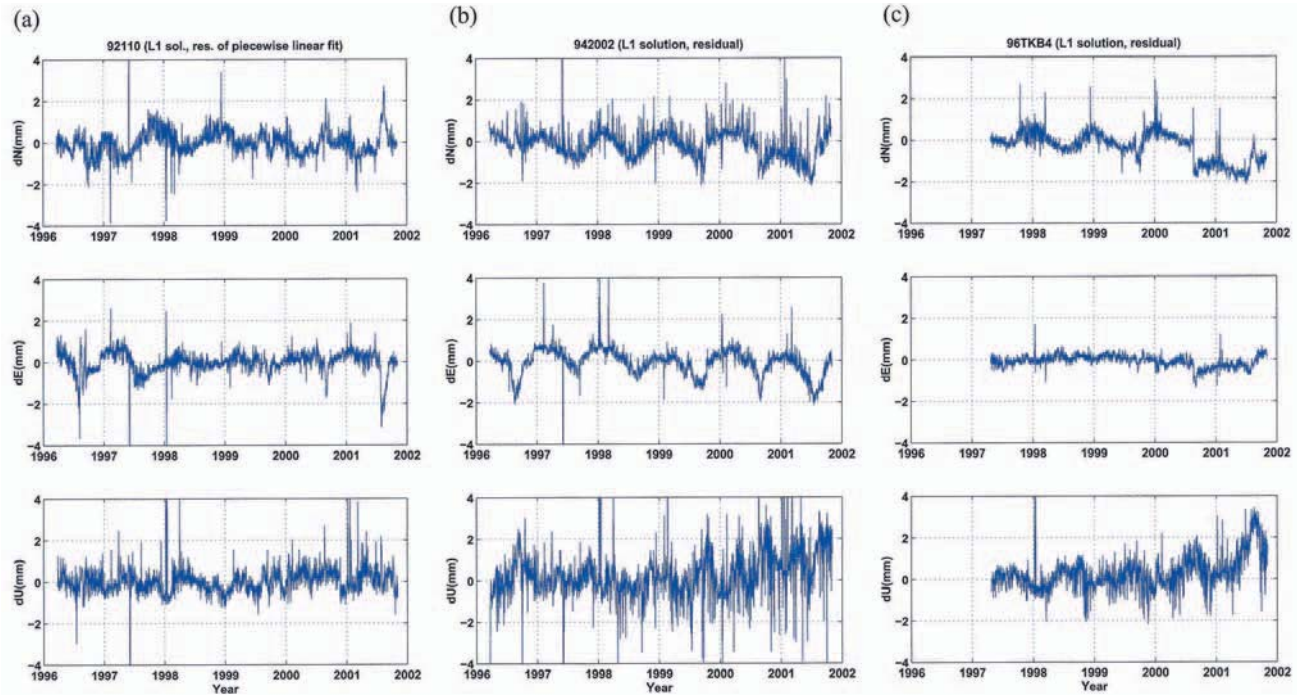

Fig. 6 Residuals of the linear (or piescewise linear) fit to the single-frequency (L1) solutions for the baselines from IGS site (TSKB) to anchor sites of three sub-networks: (a) 92110, (b) 942002, and (c) 96TKB4.

taking the velocity into account.

About 5 years of data of the Tsukuba stations are reanalyzed with the single frequency (L1) by applying the new phase maps to get the a priori coordinates and velocity for the new analysis strategy. Linear trends of the time-series of coordinates at stations 942002 (Ashtech) and 96TKB4 (Leica) are estimated. The residuals of the linear fit for the data of those stations are shown in Fig. 6 (b) and (c). Small offsets, especially in the north component, are seen both on 22 August, 2000 and in the summer of 2001, inferring episodic movements of TSKB at these timings. The former one is associated with the replacement of the antenna (IGSmail #2983). Because of these movements, the data after July, 2000 are not used for the estimation.

One of the stations (92110; Trimble) is relatively unstable and has been moving to the west by 1.5 mm/year relative to other sites. This site also moved to the northwest episodically by several millimeters in the summers of 1996 and 2001. The movement of the site was corrected by modeling the coordinate time series with a piecewise linear function. The residual of the observed time series minus the modeled ones are plotted in Fig. 6(a). The data from March, 1996 to November 11, 2001 are used for the piecewise linear fit. The movement of the TSKB site is corrected by the offset value that is estimated from the coordinate time series of 96TKB4. The offsets due to the movement of the TSKB site are, thus, not seen in Fig. 6(a).

The rms residuals of the time series fitting are summarized in Table 2. They are smaller than 0.8 millimeters except for the vertical component of 942002 which shows a larger rms of 1.3 millimeters. The velocities of the constrained sites are summarized in Table 3 for the old and new solutions. The velocity of 942002 agrees with that of 96TKB4 within 0.1 mm/year for the new results. The velocity of site 92110 in the table, which

Table 2 The rms difference of observed and modeled coordinates of stations to be constrained at Tsukuba (mm)

Station	North	East	Up	Comments
92110	0.6	0.5	0.6	Piecewise linear model
942002	0.7	0.6	1.3	
96TKB4	0.7	0.3	0.8	

Table 3 A priori velocity values of the constrained stations from the old and new solutions and their maximum differences between the sites (mm/year)

	Old solutions (ITRF96)			New solutions (ITRF97)		
Station	North	East	Up	North	East	Up
92110	-9.9	-2.9	-6.1	-12.5	-3.5	-5.2
942002	-10.9	-1.5	-5.2	-12.8	-2.1	-4.3
96TKB4	-10.9	-1.3	-4.7	-12.9	-2.0	-4.3

is for the period with no episodic movement, is slightly different from those of the other stations due to the steady movement of the site.

3.5 Reference Frame of Satellite Orbits and Earth Rotation Parameters

The reference frames are also introduced into the orbit information and the earth rotation parameters depend on the satellite orbit analysis carried out by IGS analysis centers. Several different versions of ITRF coordinate systems have been used in the history of the orbit determination analyses of IGS (Mireault, *et al*., 1999). The reference frames adopted for the IGS official products since January 1, 1994 are listed in Table 4. In the table, IGS97 and IGS00 are the IGS realizations of ITRF97 and ITRF2000, respectively, which are the reference frames realized only by the selected GPS stations so that the consistency with ITRF is held (Kouba *et al*., 1998).

In the old analysis strategy of GEONET, the IGS products were used without any transformation and thereby the reference frame was not constant with time. Moreover, the reference frames of the orbits were, in general, not consistent with those of the coordinates of the fixed stations.

Table 4 Reference frames adopted for the IGS products from 1994 to 2001

Period	Reference frame	Remarks
Jan. 1, 1994–Dec. 31, 1994	ITRF92	
Jan. 1, 1995–Jun. 29, 1996	ITRF93	
Jun. 30, 1996–Mar. 7, 1998	ITRF94	
Mar. 8, 1998–Jul. 31, 1999	ITRF96	
Aug. 1, 1998–Jun. 3, 2000	ITRF97	
Jun. 4, 2000–Dec. 1, 2001	IGS97	IGS realization of ITRF97
Dec. 2, 2001–	IGS00	IGS realization of ITRF2000

In the new analysis strategy, the IGS orbits and earth rotation parameters are transformed into ITRF97 to realize a reference frame as consistent as possible. The 7 parameters of the Helmert transformation, which count the origin shift, rotation and scale shift between the pairs of reference frames, and their rates of change, are listed in Table 5. At first, the transformation parameters are corrected for the difference in epoch. A transformation parameter at the time of observation t is obtained by

$$p(t) = p(t_0) + \dot{p} \cdot (t - t_0) \tag{1}$$

where $p(t_0)$ is the parameter at the reference epoch t_0, and $\dot{p}$ is the rate of change of the parameter. Then, the ITRFxx coordinates of the satellite positions $\mathbf{r}_{ITRFxx}$ are transformed into ITRF97 coordinates $\mathbf{r}_{ITRF97}$ by the Helmert transformation; by

$$\begin{aligned}\mathbf{r}_{ITRF97} &= \mathbf{r}_{ITRFxx} + \mathbf{T} + d \cdot \mathbf{r}_{ITRFxx} + \mathbf{R} \times \mathbf{r}_{ITRFxx} \\ &= \mathbf{r}_{ITRFxx} + \begin{bmatrix} 1 & 0 & 0 & x & 0 & z & -y \\ 0 & 1 & 0 & y & -z & 0 & x \\ 0 & 0 & 1 & z & y & -x & 0 \end{bmatrix}_{ITRFxx} \begin{bmatrix} \mathbf{T} \\ d \\ \mathbf{R} \end{bmatrix}.\end{aligned} \tag{2}$$

Here **T**, d, and **R** are the translation vector, the scale factor, and the rotation vector, respectively. The epoch of these parameters is corrected by equation (1).

The earth rotation parameters are transformed by

$$xp_{ITRF97} = xp_{ITRFxx} + R_y \tag{3}$$

$$yp_{ITRF97} = yp_{ITRFxx} + R_x \tag{4}$$

$$ut1_{ITRF97} = ut1_{ITRFxx} - R_z \tag{5}$$

Table 5 Parameters and their rates of change used for the transformation of IGS products into ITRF97

	epoch	T1(cm) (cm/yr)	T2(cm) (cm/yr)	T3(cm) (cm/yr)	S(ppb) (ppb/yr)	R1(mas) (mas/yr)	R2(mas) (mas/yr)	R3(mas) (mas/yr)
ITRF94[1)]	1999.58	0.0584 -0.05	-0.1778 -0.08	-1.3416 -0.17	0.9306 0.12	0.0306 -0.007	-0.2588 -0.005	-0.2658 0.013
ITRF96[2)]	1999.58	0.03 -0.07	0.05 0.01	-1.47 -0.19	1.43 0.19	0.159 0.013	-0.263 -0.015	-0.060 0.003
IGS00[3)]	1998.00	0.60 -0.04	0.56 -0.08	-2.01 -0.15	1.403 0.012	0.040 -0.004	-0.001 0.001	0.043 0.030

1) Those parameters are composed from parameters for IGS(ITRF94)-IGS(ITRF96) by Kouba (1998) and those for IGS(ITRF96)-IGS(ITRF97) by Springer (1999).
2) The values are taken from Springer (1999).
3) The values are taken from the IGS mail #3605. Equivalent information at the epoch 1 July 2001 is also in Ferland (2000).

where xp_{ITRFxx} and yp_{ITRFxx} are the pole coordinates and $ut1_{ITRFxx}$ is the UT1-UTC in ITRFxx coordinates. A program provided by Natural Resources Canada (IGS mail #1838; Kouba, 2002) is used for the transformation. The difference between ITRF97 and IGS97 is neglected because it is below the noise level (IGS mail #2899). The UT1 values are not given in the IGS official products from Feb. 27 to Oct. 21 of 2001. The UT1 values provided by the University of Bern (IGS mail #2751) were therefore used in the analysis for this period.

3.6 Troposphere Modeling

The signals from the GPS satellites are delayed when they pass through the neutral atmosphere. The total delay (*TD*) is the sum of the hydrostatic delay (*HD*) and wet delay (*WD*) and is modeled by using mapping functions:

$$\begin{aligned} TD(Z) &= HD(Z) + WD(Z) \\ &= ZHD \cdot M_h(Z) + ZWD \cdot M_w(Z) \end{aligned} \tag{6}$$

where *ZHD* and *ZWD* are zenith hydrostatic delay and zenith wet delay, respectively, and $M_h(Z)$ and $M_w(Z)$ are the mapping functions of hydrostatic delay and wet delay, respectively, of zenith angle *Z*. The hydrostatic mapping function is slightly different from the wet mapping function mainly because of the difference in layer thickness of dry and wet atmospheres. Zenith hydrostatic delay can be accurately estimated if surface pressure data are available (Bevis *et al*., 1992). However, default models are usually assumed in GPS analysis for a practical reason because meteorological data are not available at GPS observation sites for most cases. In the old analysis strategy, hydrostatic delay was corrected by Saastamoinen's (1973) model first. Then, the wet delay was estimated by using the mapping function of the simplified Hopfield model (Wells, 1974).

Niell (1996) developed new mapping functions by using the data of atmosphere profiles. Niell's mapping functions (NMFs) consist of two functions: one for hydrostatic delay and the other for wet delay. The NMF for hydrostatic delay has annual variation terms. The NMF values are expressed by a function of elevation angle, latitude and height of the observation sites, in addition to day of year for the hydrostatic NMF. Meteorological observation is not needed to calculate NMFs. Although NMFs are empirically derived models, they are believed to be the most accurate models at present.

In the new analysis strategy, the NMFs are used in the following way: First, hydrostatic delay is corrected by the zenith hydrostatic delay calculated by Saastamoinen's (1973) model and the NMF for hydrostatic delay. Then, the wet delay is estimated in the GPS data processing by using the NMF for wet delay.

The tropospheric gradient model (MacMillan, 1995) is used in the VLBI analysis, and several studies showed that the estimation of the gradients is effective for improving the short-term repeatability of the horizontal coordinates of GPS (Iwabuchi *et al*., 1999; Miyazaki *et al*., 1999). The implementation of such a tropospheric gradient model is, however, withheld because the network combination program of the software does not support the tropospheric gradient parameter, and remains as a pending issue until the gradient parameter is implemented in the program in future.

3.7 Other Changes Associated with the Upgrade of the Software

The version of the analysis software BERNESE was upgraded from 4.1 to 4.2. to implement the correction of ocean tide loading displacement. The other important changes associated with this upgrade are the adoption of the IERS Convention (McCarthy, 1996) for tidal models for solid earth tide, pole tide and subdaily polar motion.

The way of correction of the solid earth tide recommended by the IERS Convention (McCarthy, 1996) has two steps: The effect of the constant Love number is corrected in step 1, and the corrections for the frequency dependency of the Love number are applied in step 2. This two-step correction is implemented in version 4.2 while only the elastic case of the step 1 correction was implemented in version 4.1. Note that the restitution of permanent tide, by equation 17a,b in Chapter 7 of the IERS conventions 1996 (McCarthy, 1996), is not performed in either version 4.1 or 4.2, and thereby the obtained coordinates are consistent with the none-tidal system, in

which all the effects of the permanent tide are removed. As discussed in Chapter 3 of the IERS conventions 1996 (McCarthy, 1996), this system is different from the zero-tide system, which was recommended by Resolution 16 of the XVIII International Association of Geodesy (IAG) General Assembly in 1983.

Site displacement due to the pole tide, which is the elastic response of the earth to the polar motion, amounts to a few centimeters, depending on the place and the position of the pole (Wahr, 1985). The correction for the pole tide is also implemented in version 4.2, while it was not implemented in version 4.1.

The variation of the moment of inertia due to the tidal deformation of the earth causes a small variation of the earth's rotation (e.g. Yodar *et al*., 1981, Ray *et al*., 1994). The amplitude of the variation is in the order of 10^{-4} arcsec for pole position and 10^{-5} sec for UT1. This effect was neglected in most GPS analysis software packages until the middle of the 1990's, and so was in the old analysis strategy of GEONET. In the IERS conventions (McCarthy, 1996), a model by R. D. Ray (cited as "personal communication, 1995" in McCarthy, 1996) is recommended. This model has been applied by all IGS analysis centers since June 30, 1996 (Kouba and Mireault, 1997). The same model is adopted in the new analysis strategy.

4. Reanalysis of the GEONET Data

I compiled the data of all the GEONET stations for five and half years from March 21, 1996 and reanalyzed them with the new analysis strategy. There are 7 regional clusters (two for Ashtech and five for Trimble) at the beginning of the period, and a Leica cluster joins on April 24, 1997 when the operation of the station 96TKB4, the constrained station for the Leica sub-network, started. The number of the Ashtech clusters is fixed to two for the entire period, while it was single in the old routine analysis until March of 1997, as mentioned in the introduction.

5. Comparison of the Time Series of Coordinates and Baseline Components

Fig 7 shows examples of the time series of site

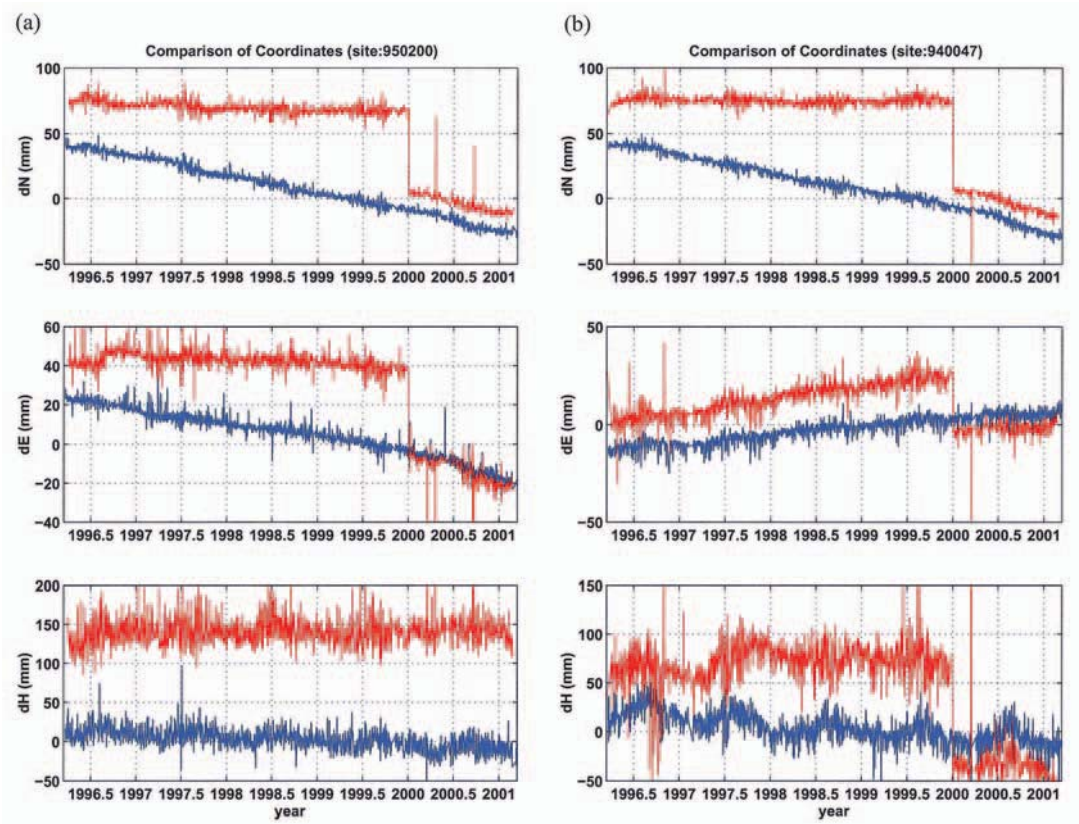

Fig. 7 Time series of the three components of the site coordinates taken from the old solution (red lines) and those from the new solutions (blue lines). The plots for Fukusima taken from the Trimble sub-network (a) and Minowa from the Ashtech sub-network (b) are shown as examples.

coordinates taken from the old and new solutions. A Trimble station (Fukushima) and an Ashtech station (Minowa) are taken as examples. The problematic features of the old solutions are evident in the coordinate time series. There are large gaps and change of trends at the beginning of the year 2000 in the old solutions shown by red curves. They are caused by the change of analysis strategies. The a priori coordinates are revised, the velocities of the constrained sites are taken into account and the Ashtech sub-network is divided into two clusters after this timing. The new solutions do not have significant gaps. The scatters of the new solutions are smaller than those of the old solutions. The improvement of precision is evident, especially, for the vertical component. The vertical component of the Minowa station shows the change of values in the middle of 1997. This seems to be caused by the increase of the number of stations in the Ashtech sub-network from 100 to 210. The effect of this change is not seen in the new solution. A change in the east component of the Fukushima station in the middle of 1996 for the old solutions is not seen in the new solutions. The number of outliers in the new solutions is smaller than that in the old solutions. Most of the outliers in the old solutions were caused by bugs in the program scripts. They are fixed in the new analysis. Note that the changes in the east component in the middle of 2000 for both stations in Fig. 7 are caused by the movement of the Tsukuba stations affected by the crustal deformation due to the seismic and volcanic activity in the Izu islands at about 200 km from Tsukuba. Because the a priori coordinates of the Tsukuba stations are not corrected for this event, the whole network is shifted to the west by 1 cm.

Fig. 8 shows examples of the time series of baseline components. The stations which form each baseline are taken from the same sub-network. Constant offsets and linear trends are estimated from the new solutions and are removed from both new and old solutions for the plots. The quality of the baseline time series is better than the coordinate time series shown in Fig. 7 even for the old solutions because the effect of changes of a priori coordinates and velocities are mostly canceled. However, these cancellations are not perfect, and there are still offsets at the beginning of the year 2000 in the old solutions; for example, in the north component of Fig.8 (a) and the vertical component of Fig. 8 (b). Another offset in the middle of the 1997 is also seen in the vertical component of Fig. 8 (b). These offsets are not seen in the new solutions. The offsets in the 1997 are also seen ambiguously in the horizontal components of Fig. 8 (b). It is hard to distinguish these offsets from linear trends within the 5 year time window. The site velocities estimated from the old solutions are, hence, slightly biased for these offsets. Note that the change in the east component in Fig. 8 (b) in the middle of 2000 is due to the movement of the Tsukuba station as mentioned in the previous paragraph.

Fig. 9 is similar to Fig. 8 except that the stations which form each baseline are taken from different sub-networks. The quality of the solutions is obviously worse than those in Fig. 8 because they are affected by inconsistency between the different sub-networks as well as error within each sub-network. Note that the vertical scales of the plots of the vertical component are nearly twice those in Fig 9. It is clear that the noise level of the new solutions is quite smaller than that of the old solutions in both the short and long terms even for the baselines between the stations from different sub-networks.

All the examples shown in this section demonstrate the improvement of the precision by the use of the new solutions. This is evaluated quantitatively in the following sections. Another important aspect of the new solutions is that their quality is quite uniform. The noises of the new solutions, such as seasonal variations, are more predictable than the old solutions. This makes it feasible to apply empirical noise models in the time-series analysis as explained in the next section.

6. Evaluation of Quality of the New Solutions

6.1 Modeling of the Baseline Time-Series

Annual variations with an amplitude of about 15 mm (max-min) are seen in the time series of the vertical coordinate of the two stations shown in Fig 7. These signals in the vertical component are commonly seen for most of the stations except for those in Tsukuba. It is plausible that the constrained sites in Tsukuba are responsible for those signals because of the similarity of the annual signals among the other stations. Since the signal is

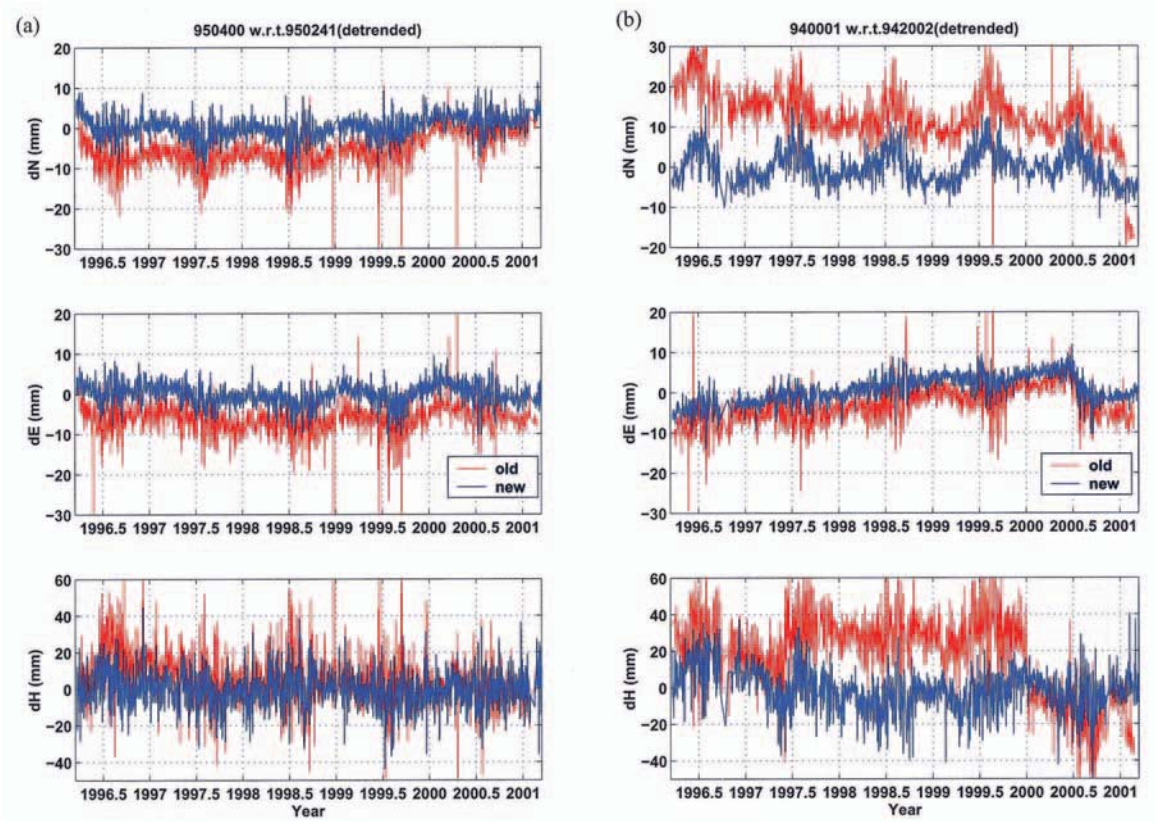

Fig. 8 Comparison of time series of baseline components taken from the old solutions (red lines) and those taken from the new solutions (blue lines). The sample baselines are taken from (a) the Trimble sub-network (Chiyoda-Oogata) and from (b) the Ashtech sub-network (Wakkanai-Tsukuba(942002)).

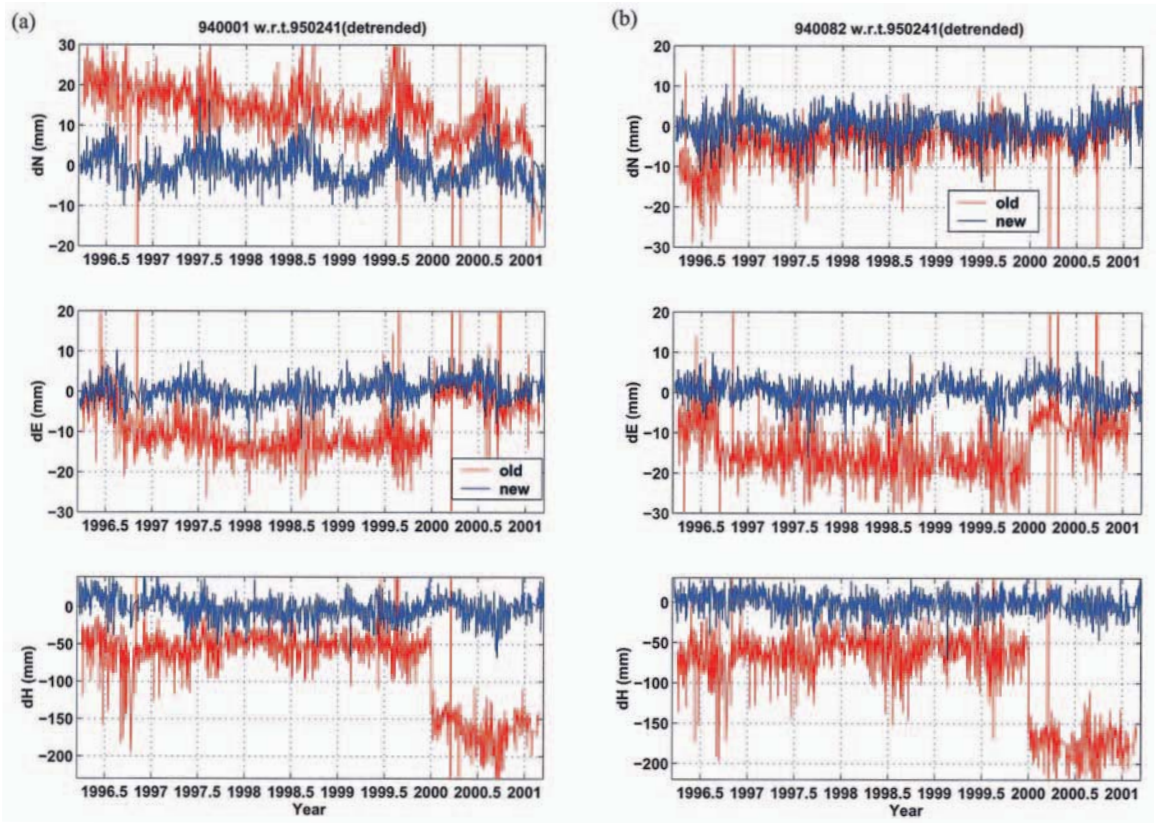

Fig. 9 Comparison of time series of baseline components taken from the old solutions (red lines) and those taken from the new solutions (blue lines). The sample baselines are taken between a Trimble site and an Ashtech site; (a) Oogata-Wakkanai and (b) Oogata-Muroto.

common to all sub-networks, it is not possible to attribute its cause only to one fixed site but all the stations in Tsukuba are commonly affected by the signal. Some local ground motions around the Tsukuba sites are thus inferred.

I eliminate this local signal for the evaluation of the time series hereafter by switching the constrained site to the Yasato station 19.1 km northeast of the Tsukuba sites. This is done by subtracting the Cartesian coordinates of the Yasato station $\mathbf{r}_{yasato}$ from those of the i-th station $\mathbf{r}_i$:

$$\mathbf{r}_{yasato} = \mathbf{r}_i - \mathbf{r}_{Yasato}. \tag{7}$$

The solution covariance matrix of the coordinates is also given for each site. The errors in the coordinates of the constrained sites are not counted in the covariance. The covariance matrices for baseline components Σ^i are calculated by adding the covariance matrix of the coordinates of the Yasato station Σ_{yasato} to those of the other stations Σ_i:

$$\Sigma^i = \Sigma_i + \Sigma_{Yasato}. \tag{8}$$

Note that this formula is valid if the correlation between the coordinates of the i-th station and those of the Yasato station is negligible. This is not exactly true for the stations that belong to the Trimble sub-network. The resulting covariance may, hence, be biased for those stations in the sense that the errors are overestimated.

The baseline time series of the i-th station $\mathbf{r}^i(t)$ is modeled by the following formulation:

$$\mathbf{r}^i(t) = \mathbf{r}^i_0 + \mathbf{v}^i \cdot (t - t_0) + \mathbf{r}^i_{seasonal}(t) + \mathbf{r}^i_{event}(t) + \varepsilon^i(t) \tag{9}$$

where $\mathbf{r}^i_0$ is the coordinates of the site at the epoch t_0 (=2000.0), $\mathbf{v}^i$ is the velocity vector, $\mathbf{r}^i_{seasonal}(t)$ is the seasonal term, $\mathbf{r}^i_{event}(t)$ is the offset term caused by seismic events, site relocation, and others, and $\varepsilon^i(t)$ is the residual of the coordinate time series.

The seasonal variation of the observed coordinate is usually asymmetrical and not well fitted by a simple cosine curve. As done by Heki (2001), this asymmetry is modeled by incorporating semi-annual terms in addition to annual terms:

$$\mathbf{r}^i_{seasonal}(t) = \sum_{n=1}^{2} \left\{ \mathbf{s}^i_n \sin\left[\frac{2\pi t}{T_n}\right] + \mathbf{c}^i_n \cos\left[\frac{2\pi t}{T_n}\right] \right\} \tag{10}$$

where T_1 (= 1 *year*) and T_2 (= 0.5 *year*) are the periods of annual and semi-annual signals, respectively, and $\mathbf{s}^i_n$ and $\mathbf{c}^i_n$ are the vector coefficients of sine and cosine terms. The asymmetrical feature of the seasonal signal is well expressed by this model.

The offsets of the time series, due to seismic events or site relocation, are modeled by step functions as follows:

$$\mathbf{r}^i_{event}(t) = \sum_k \delta\mathbf{r}^i_k H(t - t_k) \tag{11}$$

where $\delta\mathbf{r}^i_k$ is the offsets of coordinates due to the k-th event at time t_k. The offset parameters $\delta\mathbf{r}^i_k$ are set only if the offsets are visible in the coordinate time series of the site. The seismic events for which the offsets are inserted are listed in Table 6. The data during the periods of the events are not used for the estimation. Note that the periods of the slow events and earthquake swarms listed in the table are estimated only roughly because their onsets are ambiguous on the plot for most of the cases. Among those events, the slow events around the Bungo channel had taken place for more than one year, and the stations in a wide area of the Kyushu Island were affected (Ozawa, *et al*., 2001). For those stations, the 2-year data (1998-1999) are used for the estimation. It is assumed that the error term follows a normal distribution of zero-mean and that the covariance between the components is taken from the daily solutions,

Table 6 List of the seismic events for which the coordinate offsets are estimated

Date or period (DOY, Year)	Events
137-141,1996	Slow event in Boso
167, 1996	Tottori earthquake (M4.2)
224, 1996	Akita-Miyagi earthquake (M5.7)
289-292, 1996	Ito earthquake swarms
293,1996-265,1997	Slow event in Bungo channel
293, 1996	Hyuga-Nada earthquake (M6.6)
338, 1996	Hyuga-Nada earthquake (M6.6)
062-068, 1997	Ito earthquake swarms
085, 1997	Kagoshima earthquake (M6.3)
176, 1997	Yamaguchi-Shimane earthquake (M6.1)
112-129, 1998	Ito earthquake swarms
246, 1998	Iwate-san earthquake (M6.1)

and the covariance between different days is not taken into account.

The equations (9)-(11) are stated for each site and solved for the unknown parameters $\mathbf{r}^i(t_0)$, $\mathbf{v}^i$, $\mathbf{s}^i_n$, $\mathbf{c}^i_n$, and $\delta\mathbf{r}^i_k$ by applying the least-squares method by using the observed time series of site coordinates during a relatively quiet period (from March 23, 1996 to December 31, 1999). The variance-covariance matrices of the three components of the coordinate solutions are taken into account.

6.2 Long Term Repeatability

The long-term repeatability of the solutions is evaluated by the residual of the model fitting. The variance and S.D. of a component of the site coordinates for the i-th station are defined by

$$(\sigma^2)^i_p = \frac{1}{N^i - M^i} \sum_{t=1}^{N^i_t} \varepsilon^i_p(t)^2 \tag{12}$$

$$(\sigma)^i_p = \sqrt{(\sigma^2)^i_p}, \quad (p = North,\ East,\ Up), \tag{13}$$

where ε^i_p is a vector component of the residual ε^i, the subscript p indicates the component (north, east, or up), N^i and M^i are the numbers of the data points and of the estimated parameters, respectively. Similarly, the variance and S.D. for all the stations in total are defined by

$$(\sigma^2)_p = \frac{\sum_{i=1}^{N} \sum_{t=1}^{N^i} \varepsilon^i_p(t)^2}{\sum_{i=1}^{N} (N^i - M^i)} \tag{14}$$

$$(\sigma)_p = \sqrt{(\sigma^2)_p}, \quad (p = North,\ East,\ Up). \tag{15}$$

The rms residuals for the new and old solutions are mapped in Fig. 10 and Fig. 11. It is clear that the rms values for the new solutions are lower than those of the old solutions. This is confirmed by taking the variance reductions (Fig. 12). All the dots in the figure, with a few exceptions, show a significant reduction in the variances. There are clear differences in the rms values among the sub-networks for the vertical component of the old solutions: Most of the stations with larger rms than their surrounding stations in Fig. 11 (c) belong to the Ashtech sub-network. This situation is greatly improved in the new solutions (Fig. 10c). This demonstrates the homogeneity of the quality of the new solutions.

The rms residuals for the old and new solutions and the variance reductions for all the stations in total are summarized in Table 7. The rms residuals for the new

Table 7 Variance of residuals of coordinate time series

	North-south	East-west	Up-down
Old solutions	$(3.81\text{mm})^2$	$(3.83\text{mm})^2$	$(14.44\text{mm})^2$
New solutions	$(2.78\text{mm})^2$	$(2.78\text{mm})^2$	$(10.26\text{mm})^2$
Variance reduction	46.8%	47.4%	49.6%

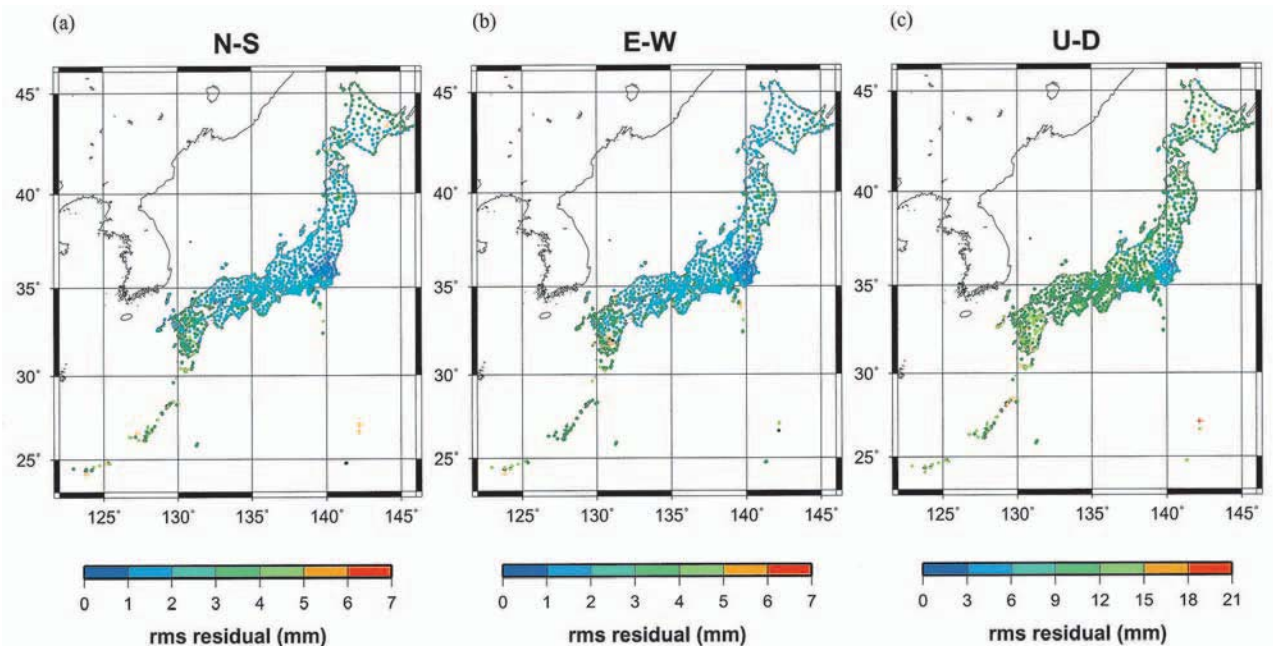

Fig. 10 RMS residuals of the time series analysis for the new solutions; north-south (a), east-west (b), and up-down (c) components.

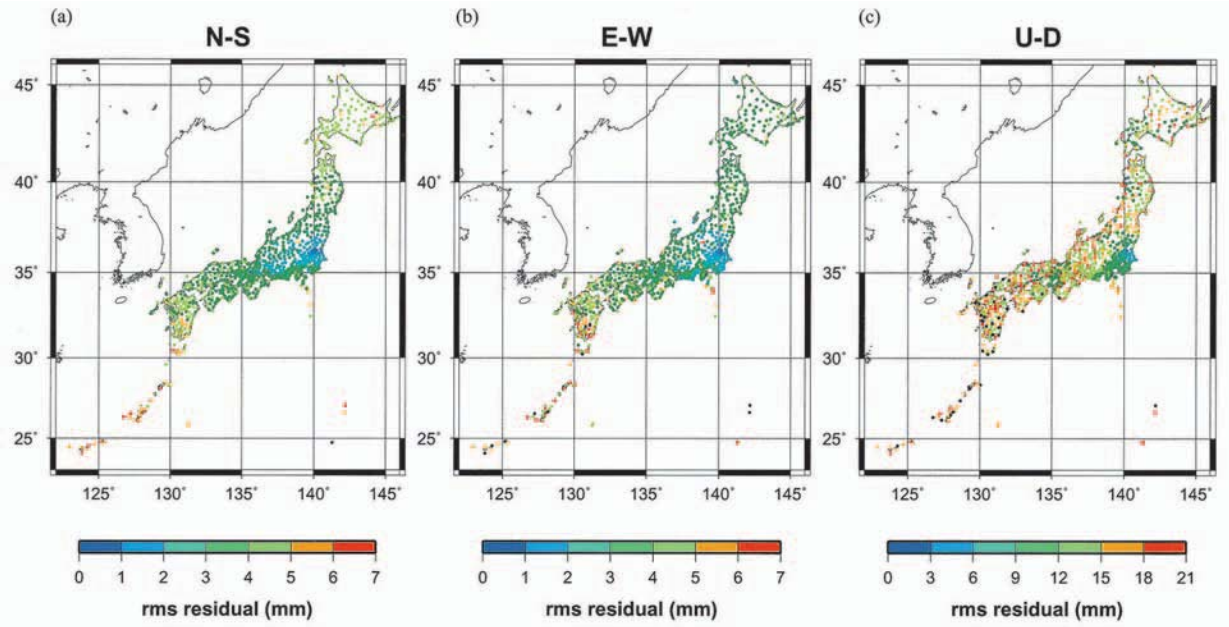

Fig. 11 RMS residuals of the time series analysis for the old solutions; north-south (a), east-west (b), and up-down (c) components. The black dots show the rms larger than the limit of the scale.

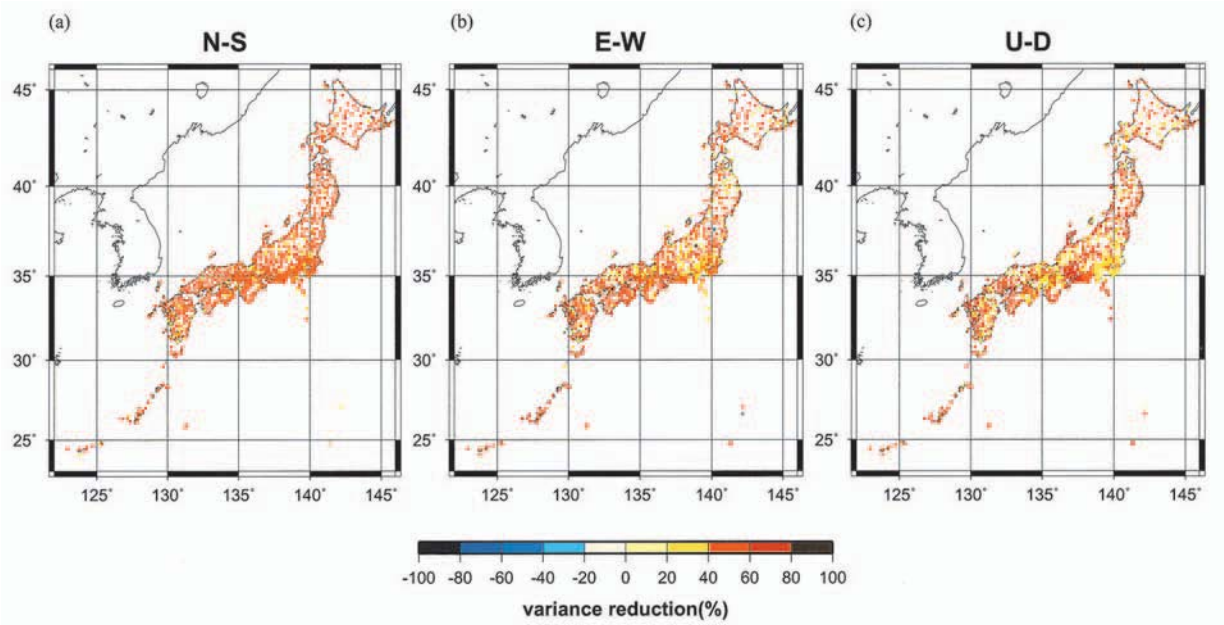

Fig. 12 The reduction of variance for each station from upgrading from the old solutions to the new solutions.

solution are less than 2.8 mm for the horizontal component and than 10.3 mm for the vertical component. It is shown in the table that the variances are reduced to a half of the old solutions (53 % for horizontal components and 50 % for the vertical component).

The rms residuals for all the stations are plotted as a function of baseline length L (slant distance from the Yasato station) in Fig. 13. The RMS residuals become larger with the increase of baseline length. It is interesting that there are bends in the trend of the plot around the baseline length of about 150 km. The S.D. values σ of each length interval (L<150 km and L > 150 km) are fitted to a linear regression model by

$$\sigma = a + b \cdot L. \tag{16}$$

The constant terms and the slopes obtained are listed in Table 8.

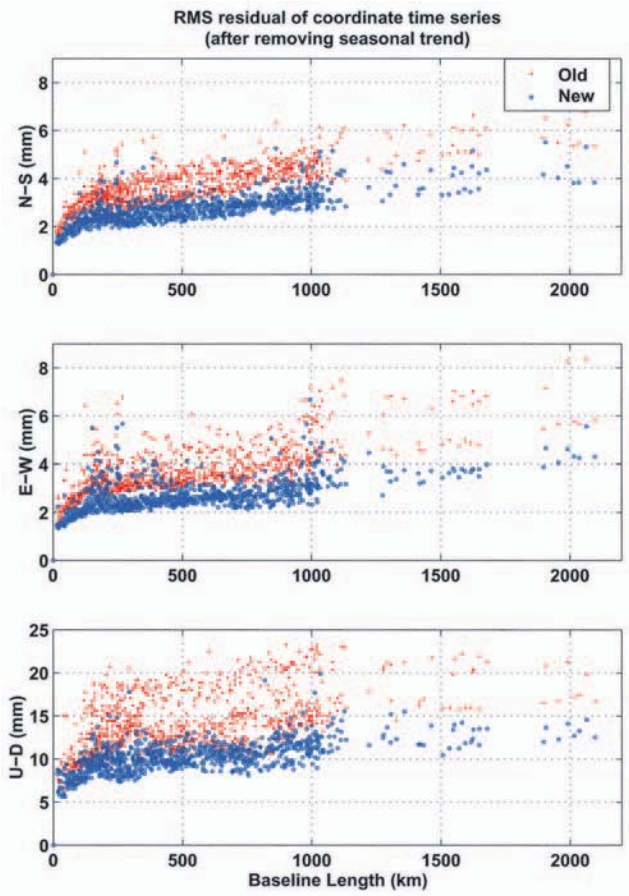

Fig. 13 RMS residuals of the time series analysis plot with the distance from the Yasato station; for the new solutions (blue dots) and for the old solutions (red dots).

Table 8 Regression coefficients for S.D. of the new solutions

components	$L < 150$ km		$L > 150$ km	
	a (mm)	b (ppb)	a (mm)	b (ppb)
North-south	1.3 ± 0.1	7.8 ± 0.6	2.2 ± 0.0	1.2 ± 0.0
East-west	1.3 ± 0.1	7.8 ± 0.7	2.3 ± 0.0	0.9 ± 0.1
Up-down	6.0 ± 0.3	22.9 ± 2.7	9.2 ± 0.1	2.4 ± 0.1

The errors in the orbit information or the earth rotation parameters are approximately proportional to the baseline length and affect over a wide area. They explain the gentle slope of the plots at distances longer than 150 km. This slope value (0.9-1.2 ppb for the horizontal component and 2.4 ppb for the vertical component) is negligibly small for ordinary applications. Eckl *et al.* (2001) also showed that the dependency of baseline length is negligible, in the case that the IGS ephemerides (final solutions) are used, by testing the accuracy of GPS baseline analysis for various baseline lengths and session durations.

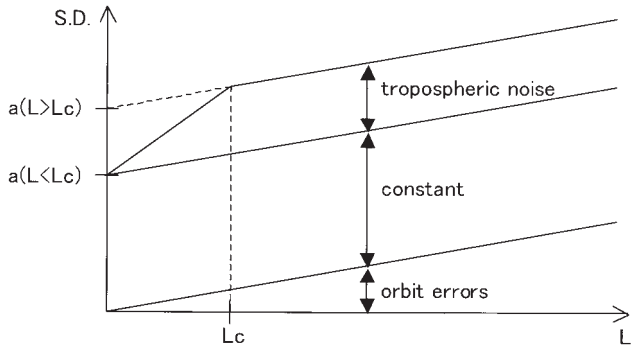

Fig. 14 Interpretation of the error factors as a function of the baseline length.

The bend of the slope at 150 km suggests the existence of noise sources that are spatially correlated within a distance shorter than this interval. Of the various error sources of GPS, tropospheric noise is the most plausible source. If this is the case, the bent distance (i.e., 150 km) is interpreted as the correlation distance L_c of the un-modeled tropospheric noise. Although the tropospheric delay is modeled with the mapping functions and estimated in the data analysis, the model may be imperfect. For example, the tropospheric gradient (MacMillan, 1995) is not modeled in the analysis, or more complicated structure of the atmosphere could affect the baseline solutions (Shimada *et al.*, 2002).

The constant term for $L < L_c$ km is interpreted as the S.D. of the localized noise or the site specific errors such as multipath or instability of the monuments, while that for $L > L_c$ km is interpreted as the S.D. of the localized noise added by an un-modeled part of the tropospheric noise which is spatially correlated within the distance of L_c (Fig 14). The variance of the noise due to the un-modeled troposphere is, therefore, estimated by taking the difference of square of those constants:

$$\sigma_t^2 = a^2(L > L_c) - a^2(L < L_c). \tag{17}$$

This variance is (1.7-1.9 mm)^2 for the horizontal components and (6.9mm)^2 for the vertical component. These values are of the same order as the constant terms $a^2(L<150)$. It is therefore inferred that the tropospheric noise is still one of the major error sources, and that the site specific or local noise also occupies a significant part of the error budget.

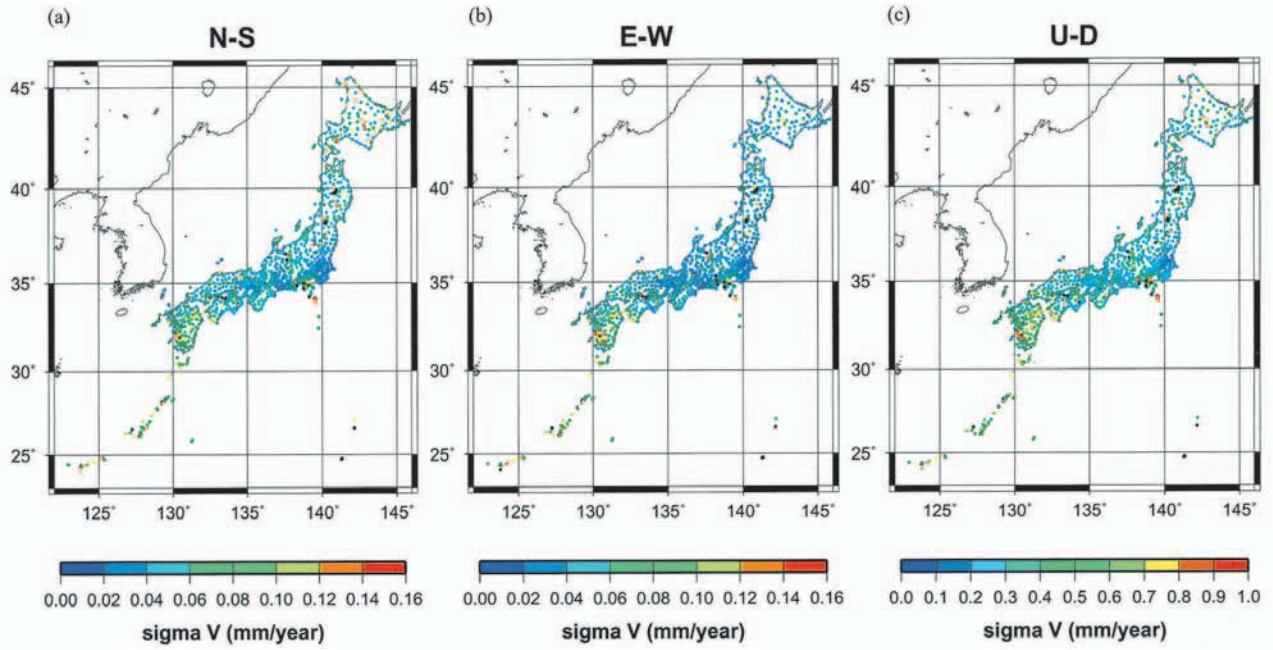

Fig. 15 The estimation error of site velocity; north-south (a), east-west (b), and up-down (c) components.

6.3 Site Velocity

The velocity vector $\mathbf{v}^i$ is a primary interest, regarding plate motion and crustal deformation. Because the data for the period from March, 1996 to December, 1999 was used, the estimated velocity is regarded as the averaged value during this period. Fig. 15 maps estimation errors of the velocity components. The errors in the velocity values of the constrained sites are not taken into account for the statistics. The medians of the sigma of the velocity are 0.056 mm/year, 0.048 mm/year, and 0.355 mm/year for the north-south, east-west, and vertical component, respectively.

The horizontal components of the velocity $\mathbf{v}^i$ obtained from the new and old solutions are mapped in Fig. 16 and Fig. 17, respectively. The velocity vectors plotted in the figures are those relative to 950241 (Ogata in Niigata prefecture). The small differences of the velocity vectors between the new and old solutions are mapped in Fig. 18. Note that the scale of vectors is 15 times larger than those of Fig. 16 and Fig. 17. The velocity differences are systematic and depend on the sub-networks and regions. Since the trends of the coordinate time series of the new solutions are more stable than those of the old solutions, as discussed in Section 5, it is most likely that the differences stem from the instability of the old solutions.

The horizontal velocity field of Japan and its implication for tectonics have been discussed by several authors based on the old solutions (e.g. Sagiya, 1999; Sagiya *et al.*, 2000; Nishimura *et al.*, 2000; Miyazaki and Heki, 2001). The differences between the new and old solutions are insignificant, and do not affect significantly the conclusions of those previous studies.

The vertical component of the crustal deformation has significant implications for many areas of earth science. It was, however, hard to use it from the old solutions because of large noise and offsets in the time series. The uniformity of the quality of the new solutions makes it possible to get the vertical velocity component accurately. Fig. 19 plots the values of the uplift rate of GEONET stations obtained from the new solutions. Because the site velocities of the Tsukuba stations are obtained based on the ITRF97 velocity of the IGS station (TSKB), the uplift rates of all the stations in the figure are given in ITRF97. It is noticeable that subsidence is dominant in a wide area of Japan. It is possible that the velocity is biased by the error in the velocity of Tsukuba in the ITRF97 solution. Table 9 lists the velocity values of the Tsukuba site taken from several versions of ITRF and transformed into the local coordinates. The velocity values of Tsukuba have changed by several mm/year at every update of the version of ITRF. Even the latest update,

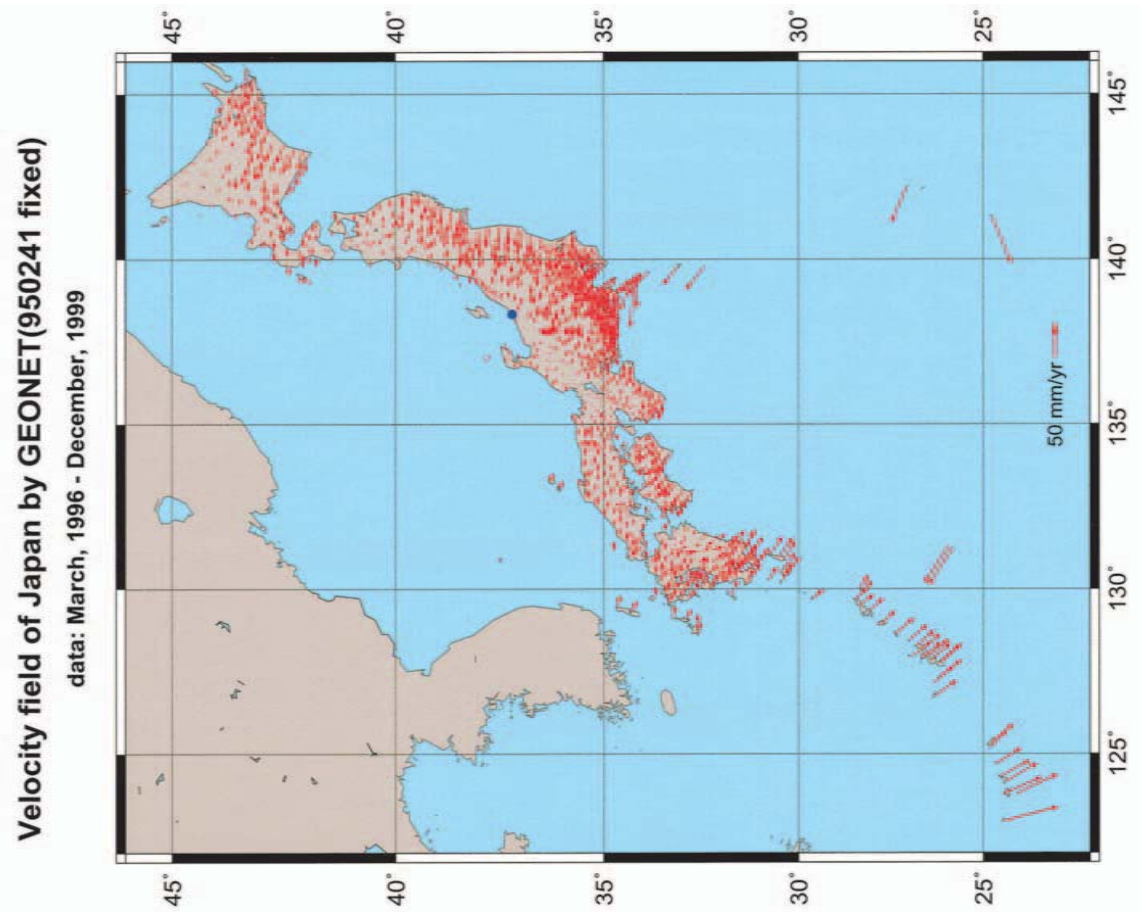

Fig. 16 Horizontal velocity of the GEONET stations derived from the new solutions from March, 1996 to December, 1999. The fixed station for the plot (Oogata) is shown by a blue dot.

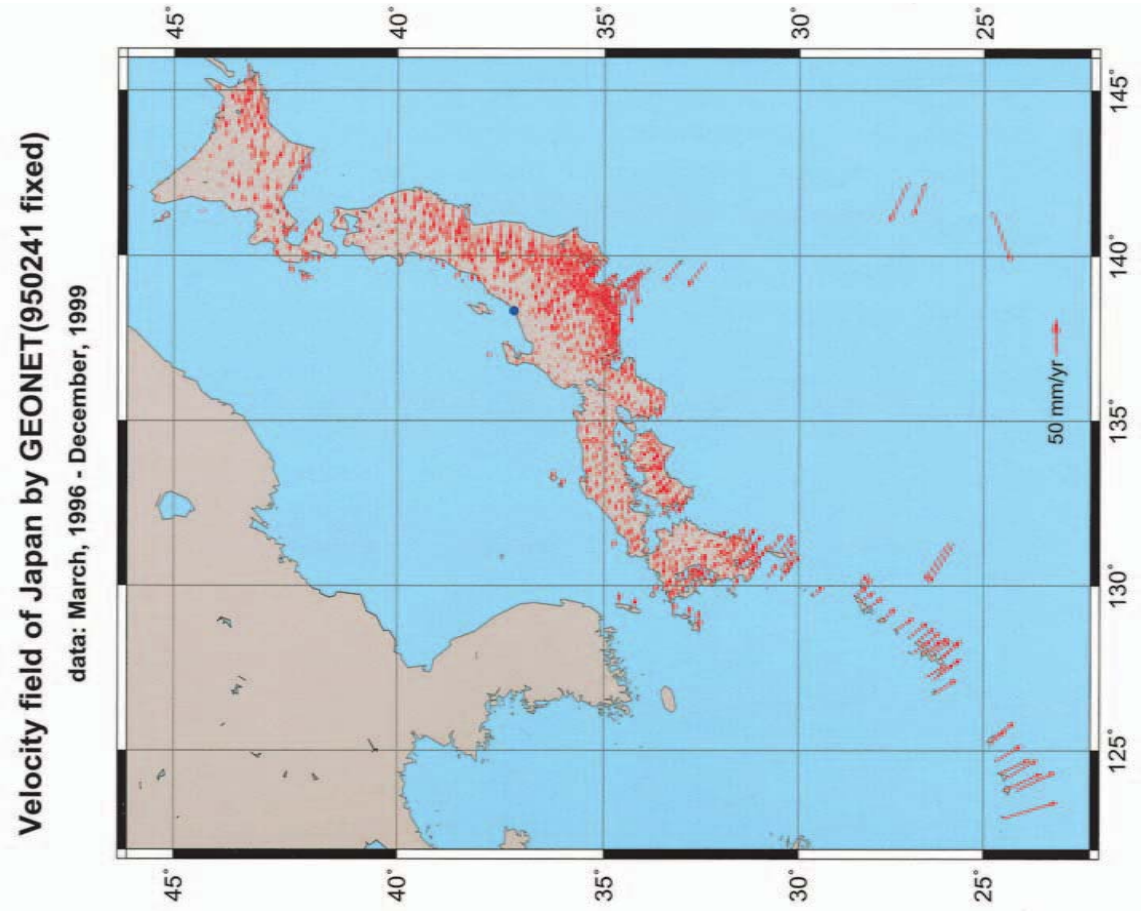

Fig. 17 Horizontal velocity of the GEONET stations derived from the old solutions from March, 1996 to December, 1999. The fixed station for the plot (Oogata) is shown by a blue dot.

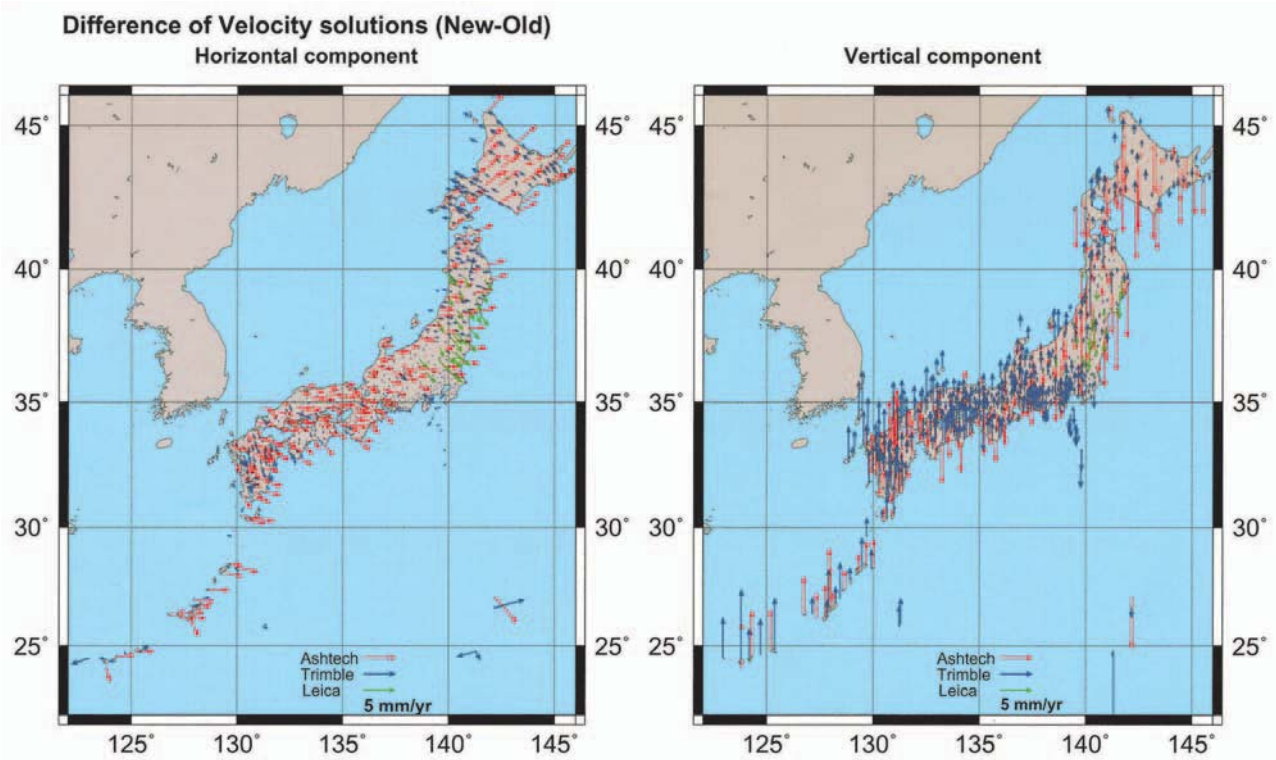

Fig. 18 Difference of the site velocities between the new and old solutions for the horizontal component (a) and the vertical component (b). The color of the arrows indicates the subnetwork to which the station belongs; Trimble (blue), Ashtech (red), and Leica (green). The upward/downward arrows in (b) indicate the change of uplift/subsidence rate from the old solution to the new solution. The differences of a priori velocities of the constrained stations (Table 3) are corrected.

Table 9 Comparison of velocity of Tsukuba site in ITRF (mm/year)

	North	East	Up
ITRF92	-11.4	0.8	-3.2
ITRF93	-16.5	3.5	0.9
ITRF93N	-7.2	1.3	0.9
ITRF94	-11.6	1.8	-2.9
ITRF96	-10.7	-1.6	-5.3
ITRF97	-12.9	-2.2	-4.4
ITRF2000	-10.3	-4.8	-0.6

from ITRF97 to ITRF2000, shows a velocity difference of 3.8 mm/year in the vertical component. The velocity field in ITRF2000 is obtained by simply adding the velocity difference of Tsukuba between ITRF2000 and ITRF97 to the velocity of each site (Fig. 20). The area of uplift and that of subsidence are more balanced in this case. This is, of course, not a proof of superiority of ITRF2000 to ITRF97. Because the velocity can be biased in either case, those values should be interpreted in a relative sense.

6.4 Comparison of GPS/PWV with Radiosonde

Ohtani and Naito (2000) evaluated the precipitable water vapors (PWVs) of 11 GEONET sites derived from the old solutions by comparing with those derived from the radiosonde data of the Japan Meteorological Agency (JMA) for a period of 10 months in 1996. They found that the GPS/PWV have a bias of –2.7 mm with a S.D. of 2.6 mm relative to the radiosonde results. Similar evaluations for the new solutions show a bias of 0.34 mm with a S.D. of 2.66mm for the same sites and period as those used by Ohtani and Naito (2000), and a bias of 1.38 mm with a S.D. of 2.54 mm for 18 sites for the 4 year period from 1996 to 1999. Nakamura *et al*. (2003) pointed out that the PWV derived from radiosonde data of JMA had a dry bias of 3-4 mm before 1999. This explains a part of the positive bias in the PWV derived from the new solutions. It also implies that the large negative bias of the GPS/PWV estimated for the old solutions (Ohtani and Naito, 2000) is even smaller than the truth. The improvement of the PWV bias is therefore significant.

7. Discussions

The improvement of the precision and accuracy,

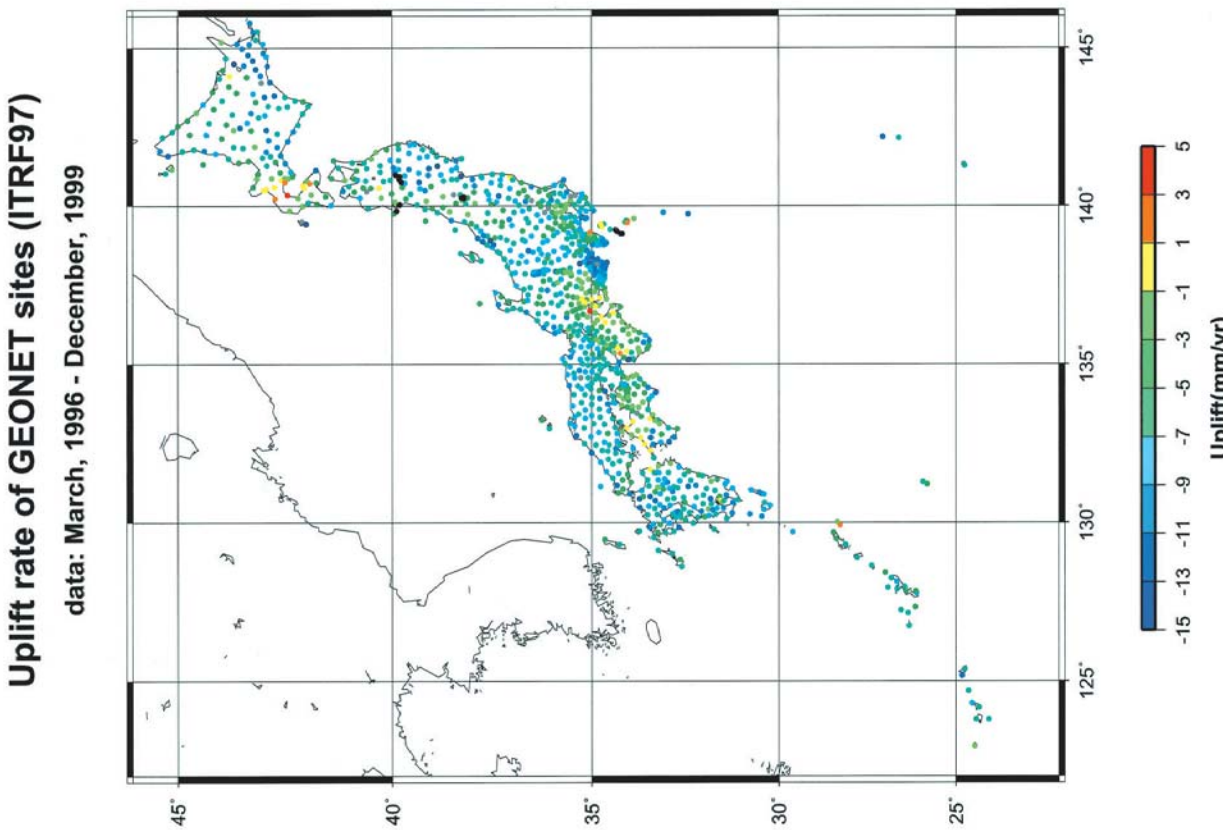

Fig. 19 Uplift rate of the GEONET stations in ITRF97 obtained from the new solutions from March 1996 to December, 1999.

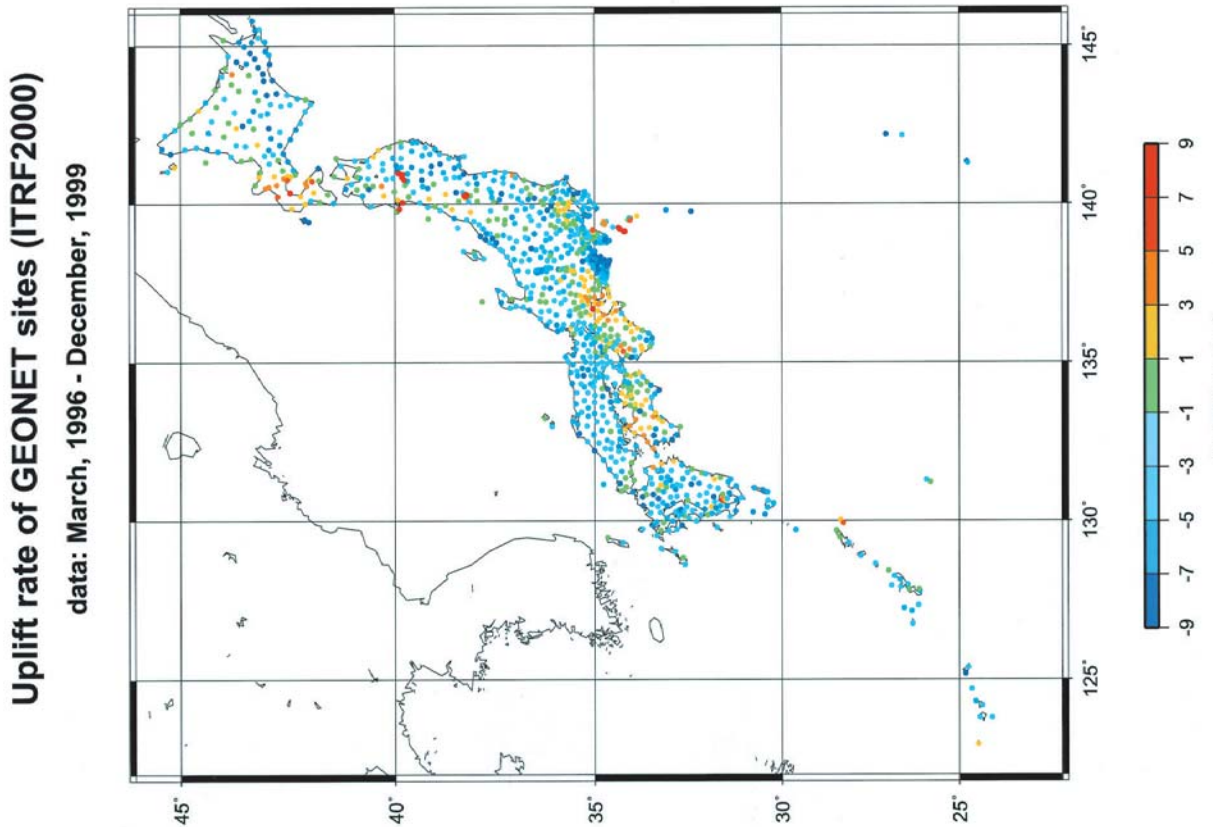

Fig. 20 Uplift rate of the GEONET stations in ITRF2000 deduced from the ITRF97 velocities shown in Fig. 19.

especially, of vertical coordinates is a major benefit of the new solutions. Features of the vertical crustal deformation of Japan are recognized in Fig. 19. A beltlike uplift zone is clearly seen from the western Tokai region to Shikoku. The eastern Tokai region (Omaezaki) is subsiding, dragged with the subducting Philippine Sea plate. The subsidence in the tips of the Kii Peninsula and the Muroto Peninsula are also explained by the same mechanism. The uplifts in the area behind the subsidence area are also associated with the subduction of the Philippine Sea plate. The Pacific coast of the eastern Hokkaido area is also subsiding, for which the effect of the subduction of the Pacific plate along the Kuril trench is inferred. The overall features of these vertical crustal movements have been also observed by leveling surveys repeatedly carried out by Geographical Survey Institute, for more than 100 years (Kunimi *et al*., 2001). The GPS data, which resolve these features by only 4-year data, significantly improve the temporal resolution, and makes it possible to discuss the temporal variation of the plate kinematics. These data, together with those of the horizontal velocity, are useful to constrain the model of interplate coupling in these regions.

Uplifts are observed at the sites close to (or on) active volcanoes or volcanic islands. Among them, the uplifts of Niijima Island and Kouzusima Island, Izu Islands, have been discussed by Polonska *et al*. (1997) and Kimata *et al*. (1999). The uplift rate of the Kouzu Island reported by Polonska *et al*. (1997) is 5 cm/year relative to the Minami-Izu station (92109) for a 10-month period from May, 1995 to February, 1996, based on GPS observation. The value of the average uplift rate for this baseline obtained in this study is 28 mm/year and is much smaller than the value reported by them. The time series of the vertical component of the baseline (Fig. 21) clearly shows the change of the rate in early 1998, which explains the discrepancy. The deceleration of the rate preceded the earthquake swarm in this region that accompanied the volcanic eruption of Miyake Island, which started at the end of June 2000. The question on the relationship between these events and the change of the rate is still open.

Observation of vertical crustal movement by the space geodetic technique is also important to resolve the global sea level change. A sea level rise of 9-88cm due to global warming is predicted for the period from 1990 to 2100 (IPCC, 2001). The rate, which is less than 2

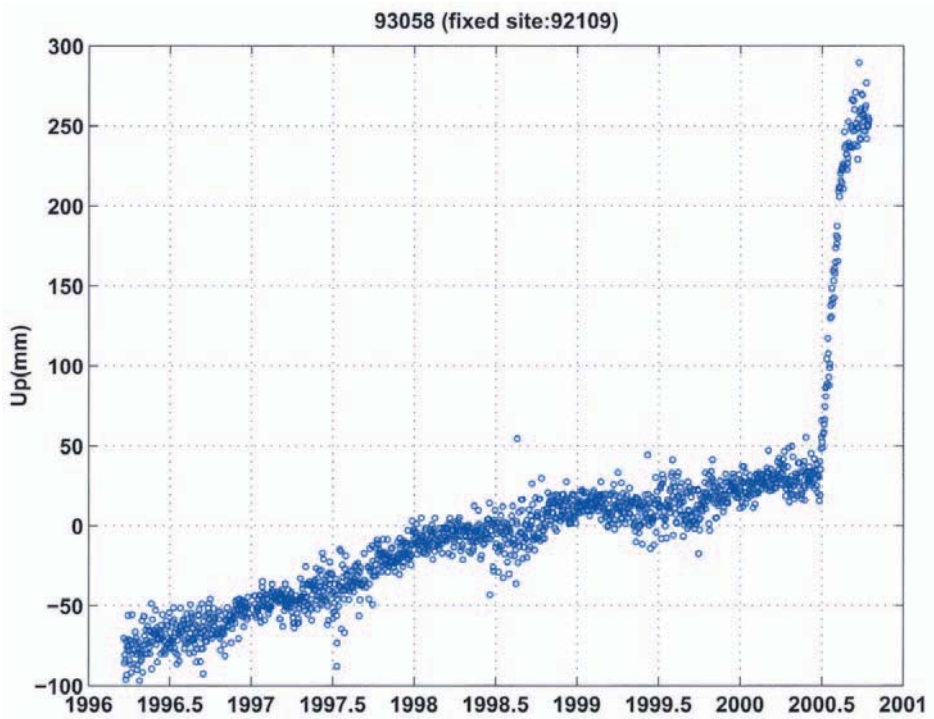

Fig. 21 The time series of vertical component of the baseline from MINAMIIZU (92109) to Kouzu (93058). The large displacement from the end of June, 2000 is due to the crustal deformation associated with the earthquake swarm that took place in this region and accompanied the eruption of the Miyake volcanic island.

mm/year for the past 100 years, is supposed to be accelerated toward the end of the 21st century. Sea level measurement at tide gage stations is one of the viable methods to detect the global sea level change. It is necessary to correct the tide gage data for the movement of the stations due to crustal deformation in order to measure the sea level change quantitatively referred to the center of the mass of the earth. As mentioned in the previous paragraph, although the relative velocity values are accurate, the absolute vertical velocities obtained in this study have an uncertainty of 3 to 4 mm/year because of the uncertainty of the velocity values of ITRF for the Tsukuba sites. This uncertainty is critically large, at present, to detect the sea level change due to global warming. Improvement of the accuracy of the ITRF value at Tsukuba is the key to detecting it by GPS networks.

The uniformity of the quality, which is also an important aspect of the new solutions, make it possible to estimate steady-state signals in the time series of the coordinates. This provides us an opportunity to investigate the seasonal signals remaining in the solutions. This can be done by further analysis of the seasonal terms (equation 10) that are already evaluated together with the site velocity. Further investigation is needed to discuss this topic which is not dealt with in this paper.

Several slow events had been detected and discussed even by using the old solutions (e.g. Ozawa, 2001). It has been proved by GEONET observation that such an event is not rare. The new solutions, which make more feasible estimating the steady-state signals precisely, will provide us more chance to detect anomalous crustal deformation as deviations from the steady-state motions and more detailed discussions of the processes of such events will be possible. Actually, Ozawa *et al*. (2002) detected a slow earthquake that began in early 2001 in the western Tokai region by a detailed analysis of the new solutions obtained in this paper. The new solutions obtained from the revised routine analysis system are vital to monitor this event, which is still continuing at the time of writing this paper.

8. Conclusions

The five years of GEONET data are reanalyzed with the new analysis strategy proposed. The new strategy solved many problems existing in the old solutions, such as the occasional changes of strategy, inconsistency between the different sub-networks, and inconsistency in the handling of reference frames. The comparison of the new solutions with the old ones shows a significant improvement, with a 50 % decrease of RMS after removing the linear and seasonal trends and the event offsets. Especially, the improvement of the precision of the vertical component is dramatic. It provides us more opportunities to use the vertical component for interpretations that were prevented by large noise in the case of the old solutions.

Another important feature of the new solutions is that the quality of the solutions is quite uniform throughout the entire period. This makes it possible to precisely estimate steady-state crustal deformation and thereby deviation from the steady state. It also provides us opportunities to investigate the noise/signals remaining in the residuals.

Acknowledgements

We would like to express our sincere gratitude to Prof. Minoru Kasahara of Hokkaido University for providing the first author the opportunity to write this paper, for his encouragement, and for his comments from an overall point of view. Prof. Kiyoshi Yomogida, Prof. Junji Koyama, and Prof. Yasunori Nishida of Hokkaido University provided valuable comments and advice. This was helpful to clarify and to quantify the points of the paper. This paper is a part of the Ph. D thesis of the first author, which was accepted by Hokkaido University in 2002. The Generic Mapping Tools (GMT, Wessel and Smith, 1998) were used to create the figures.

References

Bevis, M., S. Businger, T. A. Herring, C. Rocken, R. A. Anthes, R. H. Ware, GPS Meteorology: Remote sensing of atmospheric water vapor using the Global Positioning System, J. Geophys. Res., **97**, 15787-15801, 1992.

Brockman, E., Combination of Solutions for Geodetic and Geodynamic Applications of the Global Positioning System (GPS), Ph. D. dissertation, Astronomical Institute, University of Berne, Berne, Switzerland, 1996.

Eckl, M. C., R. A. Snay, T. Soler, M. W. Cline, G. L. Mader, Accuracy of GPS-derived relative positions as a function of interstation distance and observing-session duration., J. Geodesy, 75, 633-640, 2001.

Ferland, R., IGS Reference Frame Coordination and Working Group Activities, in "The International GPS Service 2000 Annual Report", IGS Central Bureau, the Jet Propulsion Laboratory, the California Institute of Technology, 24-27, 2000.

Gurtner, W. and G. Mader, Receiver Independent Exchange Format Version 2., CSTG GPS Bulletin Vol.3 No.3, Sept/Oct 1990, National Geodetic Survey, Rockville, 1990.

Hashimoto M., T. Sagiya, H. Tsuji, Y. Hatanaka, T. Tada, Co-seismic displacement of the 1995 Hyogo-ken Nanbu earthquake, J. Phys. Earth, **44**, 255-279, 1996.

Hatanaka, Y., H. Tsuji, Y. Iimura, K. Kobayashi, H. Morishita, Application of GPS Kinematic Method for Determination of Detection of Crustal Movements with High Temporal Resolution, in "GPS Trends in precise terrestrial, airborne, and spaceborne applications : Boulder, Colorado, USA, July 3-4, 1995", International Association of Geodesy symposia, symposium No. **115**, 105-109, 1995.

Hatanaka, Y., M. Sawada, A. Horita, and M. Kusaka, Calibration of antenna-radome and monument-multipath effect of GEONET--- Part 1: measurement of phase characteristics, Earth Planet and Space, **53**, 13-21, 2001a.

Hatanaka, Y., M. Sawada, A, Horita, M. Kusaka, J. Johnson, and C. Rocken, Calibration of antenna-radome and monument-multipath effect of GEONET---Part 2: evaluation of the phase map by GEONET data, Earth Planet and Space, **53**, 23-30, 2001b.

Hatanaka, Y., A. Sengoku, T. Sato, J. M. Johnson, C. Rocken, and C. Meertens, Detection of tidal loading signals from GPS permanent array of GSI Japan, J. Geod. Soc. Japan, 47, 187-192, 2001c.

Hatanaka, Y., Remark on Network Cluster Topology for Distributed Analysis of Wide Area GPS Networks., Technical Report, J. Geod. Soc. Japan, 2003. (accepted)

Heki, K., Seasonal modulation of interseismic strain buildup in northeastern Japan driven by snow loads, Science, **293**, 89-92, 2001.

Hugentobler, U., S. Shaer, P. Fridez (eds.), The BERNESE GPS Software Version 4.2, Astronomical Institute, University of Berne. 515 pp, 2001.

IPCC (Intergovernmental Panel on Climate Change), Climate Change 2001: The Scientific Basis : Contribution of Group I to the Third Assessment Report of the Intergovernmental Panel on Climate Change., J. T. Houghton, Y. Ding, D. J. Griggs (eds.), Cambridge University Press, Cambridge, United Kingdom and New York, NY, USA., 2001.

Iwabuchi, T., I. Naito, K. Chida, Relationship between tropospheric delay and precision of estimates of horizontal coordinates, Gekkan Chikyuu, special issue No. **25** 'Global Positioning System – evolution as an earth system sensor –' , 78-83, 1999. (In Japanese)

Iwabuchi, T., I. Naito, N. Mannouji, A comparison of Global Positioning System retrieved precipitable water vapor with the numerical weather prediction analysis data over the Japanese Islands, J. Geophys. Res., **105**, 4573-4585, 2000.

Kimata, F., S. Kariya, M. Fujita, K. Matsumoto, T. Tabei, J. Segawa, A. Yamada, Crustal movements in Kozu island, Izu islands in southern central Japan, detected by GPS measurements (July, 1996-November 1997), Volcano, **44**, 13-22, 1999. (in Japanese)

King, R. W. and Y. Bock, Documentation of the GAMIT GPS analysis software Ver. 9.3, Mass. Institute of Technology and Scripps Institute of Oceanography, 1994.

Kouba, J., Analysis Activities, in "The International GPS Service 1998 Annual Report", IGS Central Bureau, the Jet Propulsion Laboratory, the California Institute of Technology, 13-17, 1998.

Kouba, J. and Y. Mireault, Analysis Coordinator Report, 1996 IGS Annual Report, 55-100, 1997.

Kouba, J., J. Ray, M. M. Watkins, IGS reference frame realization, Proceedings of 1998 IGS Analysis Center Workshop, Darmstadt, Germany, Europian Space Agency, 139-171, 1998.

Kouba, J., ITRF Transformations, The GPS Toolbox, GPS Solutions, 5(3), 88-90, 2002.

Kunimi, T., Y. Takano, M. Suzuki, T. Saito, T. Narita, S.

Okamura, Vertical Crustal Movements in Japan Estimated from the Leveling Observations Data for the Past 100 Years, Journal of the Geographical Survey Institute, **96**, 23-37, 2001. (in Japanese)

MacMillan, D. S., Atmospheric gradients from very long baseline interferometry observations, Geophys. Res. Lett., 22, 1041-1044, 1995.

McCarthy D. D., IERS conventions (1996), IERS Technical Note 21, Central Bureau of IERS, Observatoire de Paris, Paris, 1996.

Matsumoto, K., T. Takanezawa, and M. Ooe, Ocean tide models developed by assimilating TOPEX/POSEIDON altimeter data into hydrodynamical model: A Global Model and a Regional Model Around Japan, Journal of Oceanography, **56**, 567-581, 2000.

Matsumoto, K., T. Sato, T. Takanezawa, and M. Ooe, GOTIC2: A program for computation of oceanic tidal loading effect., J. Geod. Soc. Japan, **47**, 243-248, 2001.

Mireault, Y., J. Kouba, J. Ray, IGS Earth rotation parameters, GPS Solutions, **3**, 59-72, 1999.

Miyazaki, S., H. Tsuji, Y. Hatanaka, Y. Abe, A. Yoshimura, K. Kamada, K. Kobayashi, H. Morishita, Y. Iimura, Establishment of the nationwide GPS array (GRAPES) and its initial results on the crustal deformation of Japan, Bulletin of Geographical Survey Institute, **42**, 27-41, 1996.

Miyazaki, S., T. Saito, M. Sasaki, Y. Hatanaka, Expansion of GSI's nationwide GPS array, Bulletin of Geographical Survey Institute, **43**, 23-34, 1997.

Miyazaki, S., T. Iwabuchi, T., I. Naito, Estimation of tropospheric gradients and improvement of the precision of horizontal coordinates, Gekkan Chikyuu, special issue No. **25** 'Global Positioning System – evolution as an earth system sensor –' , 84-90, 1999. (In Japanese)

Miyazaki, S., K. Heki, Crustal velocity field of southwest Japan: Subduction and arc-arc collision, J. Geophys. Res., **106**, 4305-4326, 2001.

Murakami, M., S. Miyazaki, Periodicity of strain accumulation detected by permanent GPS array: possible relationship to seasonality of major earthquakes' occurrence, Geophys. Res. Lett., **28**, 2983-2986, 2001.

Nakamura, H., H. Seko, Aerological Observatory, Meteorological Instruments Center, Dry Bias of Humidity Measurements by Rawinsondes Revealed by the Comparison with GPS Derived Precipitable Water Vapor, Proceedings of International Workshop on GPS Meteorology, Tsukuba, 2003.

Niell, A., Global mapping functions for the atmosphere delay at radio wave lengths, J. Geophys. Res., **100**, 3227-3246, 1996.

Nishimura, T., S. Miura, K. Tachibana, K. Hashimoto, T. Sato, S. Hori, E. Murakami, T Kono, K. Nida, M. Mishima, T. Hirasawa, S. Miyazaki, Distribution on the subducting plate boundary in northeastern Japan inferred from GPS observations, Tectonophysics, **323**, 217-238, 2000.

Ohtani, R., and Naito, I. Comparisons of GPS-derived precipitable water vapors with radiosonde observations in Japan, J. Geophys. Res., **105**, 26,917-26,930, 2000.

Ozawa, S., M. Murakami, T. Tada, Time-dependent inversion study of the slow thrust event in the Nankai trough subduction zone, southwestern Japan, J. Geophys. Res., **106**, 787-802, 2001.

Ozawa, S, M. Murakami, M. Kaidzu, T. Tada, T. Sagiya, Y. Hatanaka, H. Yarai, and T. Nishimura, Detection and Monitoring of Ongoing Aseismic Slip in the Tokai Region, Central Japan, Science, **298**,1009-1012, 2002.

Polonska, D., M. Harigae, T. Tsujii, M. Murata and F. Kimata, Observed vertical motion of Kozu-Jima Island using interferometric GPS., Technical Report of National Aerospace Laboratory, TR-1322T, 1-9, 1997.

Ray, R. D., D. J. Steinberg, B. F. Chao, D. E. Cartwright, Diurnal and semidiurnal variations in the earth's rotation rate induced by oceanic tides, Science, **264**, 830-832, 1994.

Saastamoinen, I. I., Contribution to the theory of atmospheric refraction, Bulletin Geodesique, **107**, 13-34, 1973.

Sagiya, T., A. Yoshimura, E. Iwata, K. Abe, I. Kimura, K. Uemura, T. Tada, Establishment of permanent GPS observation network and crustal deformation monitoring in the southern Kanto and Tokai Areas, Bulletin of Geographical Survey Institute, **41**, 105-118, 1995.

Sagiya, T., Intraplate coupling in the Tokai district, central Japan, deduced from continuous GPS data, Geophys. Res. Lett., **26**, 2315-2318, 1999.

Sagiya, T., S. Miyazaki, T. Tada, Continuous GPS array and present-day crustal deformation of Japan, PAGEOPH, **157**, 2303-2322, 2000.

Sagiya, T., Searching for Silent Earthquakes with Geodetic Data, Bulletin of Geographical Survey Institute, **48**, 25-38, 2002.

Shimada, S., H. Seko, H. Nakamura, K. Aonashi, and T. A. Herring, The impact of atmospheric mountain lee waves on systematic geodetic errors observed using the Global Positioning System, Earth Planets Space, **54**, 425-430, 2002.

Springer, T., Analysis Activities, in "The International GPS Service 1999 Annual Report", IGS Central Bureau, the Jet Propulsion Laboratory, the California Institute of Technology, 12-16, 1999.

Tsuji, H., Y. Hatanaka, T. Sagiya, M. Hashimoto, Coseismic crustal deformation from the 1994 Hokkaido-Toho-Oki earthquake monitored by a nationwide continuous GPS array in Japan, Geophys. Res. Lett., **22**, 1669-1672, 1995.

Yoder, C. F., J. G. Williams, M. E. Parke, Tidal variations of earth rotation, J, Geophys. Res., **86**, 881-891, 1981.

Wahr, J. M., Deformation induced by polar motion, J. Geophys. Res., **90**, 9363-9368, 1985.

Webb, F. H., and J. F. Zumberge, An introduction to the GIPSY/OASIS-II, JPL publ. D-11088, Jet Propulsion Laboratory, California Institute of Technology, Pasadena, California, 1993.

Wells, D. E., Doppler satellite control, Department of Surveying Engineering, University of New Brunswick, Fredericton, N. B., 1974.

Wessel, P. and W. H. F. Smith, New, improved version of the Generic Mapping Tools released, EOS Trans. AGU, **79**, 579, 1998.

Wu, J. T., S. C. Wu, G. A. Hajj, W. I. Bertiger, S. M. Lichten. Effects of antenna orientation on GPS carrier phase. Manuscripta Geodaetica **18**, 91-98, 1993.

Appendix Specification of the New Analysis Strategy

MEASUREMENT MODELS	
Preprocessing	Phase preprocessing in a baseline-by-baseline mode using triple-differences. In most cases cycle slips are fixed looking simultaneously at different linear combinations of L1 and L2. If a cycle slip cannot be fixed reliably, bad data points are removed or new ambiguities are set up.
Basic Observable	Carrier phase, code only used for receiver clock synchronization. Elevation angle cutoff : 15 degrees Sampling rate : 2 minutes Weighting : 1.2 cm for double-diff. ionosphere-free LC. : elevation-dependent weighting function $1/\cos^2 Z$
Modeled Observable	Double-differences, ionosphere-free linear combination
RHC phase rotation correction	Phase polarization effects applied (Wu *et al.*, 1993)
Ground antenna phase center calibrations	Elevation-dependent phase center corrections are applied according to the model GSI_01 (Hatanaka, *et al.*, 2001a) The corrections are given relative to the Dorne Margolin T antenna.
Troposphere	A priori model : Dry terms are given by Saastamoinen (1973) model with Niell(1996) dry mapping function.
	Met data input : none
	Estimation : zenith wet delays in 3 hour with the piecewise constant model. Tropospheric gradient parameters are not estimated.
	a priori sigma : 9.99 m for absolute value : 9.99 m for relative value
	Mapping function : Niell mapping function (Wet) (Niell, 1996)
Ionosphere	Not modeled (Ionospheric delays are eliminated by forming the ionosphere-free linear combination of L1 and L2).
Tidal displacements	Solid earth tidal displacement: complete model from IERS Conventions 1996 (McCarthy, 1996)
	Permanent tidal term : not included in site coordinates (consistent with the non-tidal crust system)
	Step 1: in-phase: degree 2 and 3 Nominal h02 and l02 : 0.6078, 0.0847 (anelastic) Nominal h22 and l22 : -0.0006, 0.0002 Nominal h3 and l3 : 0.292 , 0.015 out-of-phase: degree 2 only semi- and diurnal diurnal: nominal hI, lI : -0.0025,-0.0007 semi-di: nominal hI, lI : -0.0022,-0.0007 latitude dependence diurnal : nominal l1 : 0.0012 semi-di : nominal l1 : 0.0024 Step 2: in-phase: degree 2, diurnal in-phase and out-of-phase: long-period tides
	Pole tide correction: applied (McCarthy, 1996) nominal mean m1, m2 : 0.033, 0.331 arcsec.
	Ocean loading: Amplitudes and phases of major 11 constituents calculated by GOTIC2 software (Matsumoto *et al.*, 2001) with Matsumoto *et al.* (2000)'s model.
Atmospheric loading	Not applied
Earth orientation models (EOP)	Subdaily EOPs : RAY model applied (McCarthy, 1996)
Satellite center of mass correction	Block I x,y,z : 0.2100, 0.0000, 0.8540 m Block II/IIA x,y,z : 0.2794, 0.0000, 1.0230 m Block IIR x,y,z : 0.0000, 0.0000, 0.0000 m
Satellite phase center calibration	Not applied
Relativity corrections	Periodic, -2(R*V/c) : applied Gravity bending : not applied Dynamical : applied (McCarthy, 1996, Ch.11, Eq.1)
GPS attitude model	Not applied

ESTIMATED PARAMETERS (APRIORI VALUES & SIGMAS)	
Adjustment	Weighted least-squares algorithms
Station coordinates	One station for each of 3 sub-networks is constrained with a priori sigma of 0.1 mm, the remaining stations estimated. The list of constrained sites: 92110 : Trimble sub-network 942002 : Topcon sub-network 96TKB4 : Leica sub-network When the data of the above stations are not available, the nearest station in the sub-network is constrained.
Troposphere	Zenith delays estimated once per 3 hours for each station. Loosely constrained to 9.99 meters.
Ambiguity	Ambiguities are resolved in a single baseline mode in two steps: L5 (Widelane) ambiguities are resolved first, and L1 & L2 ambiguities second.

REFERENCE FRAMES	
Orbit & Earth rotation parameters	IGS final products are used transformed to ITRF97 by Helmert transformation.
Terrestrial	ITRF97 reference frame: constraints (0.1 mm) on the coordinates and velocities of one site for each sub-network. Coordinate and velocity values given in the ITRF97 tied from the IGS station (TSKB). The antenna heights are set to zero, which means that the coordinates in the solutions point to the antenna reference point (antenna bottom for the Trimble and TOPCON sites, 45 mm below the antenna bottom for Leica AT303 sites.)

DISTRIBUTED ANALISYS AND NETWORK COMBINATION STRATEGY	
METHODOLOGY	NORMAL EQUATION STACKING (Brockmann, 1996)
Network	Terminology for the network hierarchies: - the whole network - sub-networks - clusters - units - sites
Sub-network	Whole network is divided into following sub-networks: - Trimble sub-network : - Topcon (Ashtech) sub-netwok : - Leica sub-network : The sites are classified into the above 3 sub-networks according to the site specification before the year 2001. This classification is fixed, although the receivers are changed for some of the sites in 2001. Each sub-network is solved independently.
Cluster	- The Trimble sub-network is divided into 5 regional clusters and backbone cluster. The backbone cluster contains at least 3 anchor sites from each regional cluster. - The Topcon sub-network is divided into 2 clusters each of which contains the fiducial site at Tsukuba (942002). - The Leica sub-network consists of just a single cluster.
Unit	Each cluster, except for the backbone cluster, is divided into small units that consist of about 20 sites. One site from each unit is taken and summarized into a special unit that is used to link the units into a cluster.
Combination 0	At the beginning of the network combination, the NEQ file of each unit is provided by phase processing with the ambiguity parameters eliminated. There are only coordinate and tropospheric parameters in the NEQ files.
Combination 1	Combination step 1: units → cluster - The Normal Equation (NEQ) files are combined within each regional cluster. The backbone cluster is also combined with each regional cluster for the Trimble sub-network. - The tropospheric parameters are eliminated after output to the files. - The NEQ file for each regional cluster is output.
Combination 2	Combination step 2: clusters → sub-networks - The NEQ files of regional clusters are combined into sub-networks. - Each sub-network is constrained at the sites in Tsukuba. - The final set of site coordinates are obtained.